IEEE Standards

IEEE Std 356™-2001
(Revision of IEEE Std 356-1974)

356™

IEEE Guide for Measurements of Electromagnetic Properties of Earth Media

IEEE Antennas & Propagation Society

Sponsored by the
Wave Propagation Standards Committee

IEEE

Published by
The Institute of Electrical and Electronics Engineers, Inc.
3 Park Avenue, New York, NY 10016-5997, USA

3 June 2002

Print: SH94971
PDF: SS94971

Recognized as an
American National Standard (ANSI)

IEEE Std 356™-2001
(Revision of IEEE Std 356-1974)

IEEE Guide for Measurements of Electromagnetic Properties of Earth Media

Sponsor

Wave Propagation Standards Committee
of the
IEEE Antennas & Propagation Society

Approved 2 May 2002
American National Standards Institute

Approved 10 October 2002
IEEE-SA Standards Board

Abstract: The electromagnetic properties of the earth play an important role in the design and implementation of radio communications systems, geophysical prospecting instruments, and subsurface mapping techniques. Measurement techniques include dc resistivity, surface impedance, propagation studies, wave tilt methods, probe impedance methods, mutual impedance methods, transient methods, time domain reflectometry, ground probing radar, laboratory-based techniques, and free-space reflection measurements. The separation distance between the probes and the wavelength of the radiation both affect the volume of earth material measured. This guide provides a summary of current measurement techniques and, where appropriate, inversion methods for determining the conductivity and the relative permittivity of the volume under investigation.
Keywords: dc resistivity, earth permittivity measurements, electromagnetic geophysics, ground conductivity measurements, ice, inversion, radio communications, radio reflection, surface impedance, time domain reflectometry

The Institute of Electrical and Electronics Engineers, Inc.
3 Park Avenue, New York, NY 10016-5997, USA

Print: ISBN 0-7381-3084-2 SH94971
PDF: ISBN 0-7381-3085-0 SS94971

At the time of approval of this guide, the IEEE Antennas & Propagation Society (AP-S) Wave Propagation Standards Committee (WPSC), which balloted and approved this guide for submission to the IEEE Standards Board, had the following membership:

Wolfhard J. Vogel, *Chair*

George H. Hagn, *Secretary*

Richard W. Adler	Walter A. Flood	Warren S. Stutzman
Gary S. Brown	Motohisa Kanda	David V. Thiel
John F. Cavanagh	Ernest K. Smith	Fawwaz T. Ulaby
Warren Flock	Glenn S. Smith	John C. H. Wang

The subcommittee, the WPSC, and the AP-S appreciate the assistance of all those who contributed to this guide.

The following members of the balloting group voted on this guide. Balloters may have voted for approval, disapproval, or abstention.

Richard W. Adler	Peter Flanagan	W. Ross Stone
E. Robert Bonsen	Mark F. Hutchins	David V. Thiel
Charles A. Cooper	John Lepore	Wolfhard J. Vogel
Ernest M. Duckworth, Jr.		Larry S. Young

When the IEEE-SA Standards Board approved this guide on 7 December 2001, it had the following membership:

Donald N. Heirman, *Chair*

James T. Carlo, *Vice Chair*

Judith Gorman, *Secretary*

Satish K. Aggarwal	James H. Gurney	James W. Moore
Mark D. Bowman	Richard J. Holleman	Robert F. Munzner
Gary R. Engmann	Lowell G. Johnson	Ronald C. Petersen
Harold E. Epstein	Robert J. Kennelly	Gerald H. Peterson
H. Landis Floyd	Joseph L. Koepfinger*	John B. Posey
Jay Forster*	Peter H. Lips	Gary S. Robinson
Howard M. Frazier	L. Bruce McClung	Akio Tojo
Ruben D. Garzon	Daleep C. Mohla	Donald W. Zipse

*Member Emeritus

Also included are the following nonvoting IEEE-SA Standards Board liaisons:

Alan Cookson, *NIST Representative*
Donald R. Volzka, *TAB Representative*

Savoula Amanatidis
IEEE Standards Managing Editor

Contents

IEEE Guide for Measurements of Electromagnetic Properties of Earth Media

1. Overview

The electromagnetic properties of the earth (conductivity σ in S/m, permittivity ε in F/m, and magnetic permeability μ in H/m) can have a major effect on the performance of electrical and electromagnetic systems. Examples of these systems include both communications systems and remote sensing systems. For example, the electrical properties of the earth beneath an antenna can influence the antenna efficiency (and the need for a metallic ground plane) and radiation pattern, and these properties also can limit the effective depth of ground-penetrating radar. Many different methods and techniques have evolved for the measurement of the electrical properties of the earth at and near the surface at radio frequencies, and other methods using lower frequencies were developed for measuring the conductivity deeper into the earth for geophysical prospecting and other applications.

This guide is intended to describe these methods (both the theory and field methodology) and provide references for further reading for each method. The descriptions represent the recommended practice of these techniques. There is a further attempt to provide guidance on the limits of applicability of the methods (e.g., in frequency or in geographical context).

This guide has been prepared by the Wave Propagation Standards Committee of the IEEE Antennas & Propagation Society to replace IEEE Std 356-1974, IEEE Guide for Radio Methods of Measuring Earth Conductivity [B1.7],[1] which was also published as a paper by deBettencourt et al. [B1.5]. In 1974 Lytle published a comprehensive review paper [B1.14].

The International Telecommunication Union (ITU) has published world surface conductivity maps for a number of frequency bands [B1.9], although these are no longer being updated. The curves of conductivity and relative permittivity in ITU-R Recommendation 527-3 [B1.8] exhibit no dispersion in the band 3–30 MHz, whereas measured values show significant dispersion in this band for which surface soils typically can show characteristics from lossy conductors to lossy dielectrics [B1.11]. The real and imaginary parts of the complex relative permittivity form a Hilbert transform pair. As a result, the conductivity and relative permittivity are not independent variables. Their mutual coupling

[1]The numbers in brackets correspond to those of the bibliography in Annex B.

is described by the Kramers–Kronig relations [B1.11]. Therefore, the ITU values for the HF band are inconsistent with the results of complex variable theory and are in error.

1.1 Scope

The purpose of this guide is to describe the measurement principles of the electrical properties of naturally occurring solid materials, although it will also serve as a guide for the measurement of any solid material. These properties are the conductivity σ (in S/m) and the permittivity (or dielectric constant) ε (in F/m). The magnetic permeability μ (in H/m) will not be considered except where it impacts on the interpretation. This is because $\mu \cong \mu_0$ (to within less than 5%) for most naturally occurring materials. Even dry, pure magnetite sand only increases μ_r to 1.09. In free space (vacuum), the permittivity is $\varepsilon_0 = 8.854 \times 10^{-12}$ F/m and the magnetic permeability is $\mu_0 = 4\pi \times 10^{-7}$H/m.

The conductivity of a material is defined by Ohm's Law; i.e., the current I (in A) passing through a block of the material (length l in m and cross-section A in m^2) is related to the voltage V applied to plate electrodes covering two parallel faces of the cube, as given by Equation (1):

$$I = \frac{V}{R} \tag{1}$$

where R is the resistance in ohms. The conductivity σ can be determined using Equation (2):

$$R = \frac{l}{\sigma A} \tag{2}$$

Similarly, the permittivity of the material can be determined by the same physical arrangement of a block (area A and length l) between two parallel electrodes by measuring the voltage V between the plates and the charge stored on the plates Q (in coulombs) by the capacitance C (in F/m), as shown by Equation (3) and Equation (4):

$$C = \frac{Q}{V} \tag{3}$$

and

$$C = \frac{\varepsilon A}{l} \tag{4}$$

where the effects of fringing fields have been ignored. The similarity between the measurements of R and C, and consequently ε and σ, result in very similar methods being used to determine the two parameters.

In particular, by using Equation (5), one can write [B1.3]:

$$RC = \frac{\varepsilon}{\sigma} \tag{5}$$

When the material has conduction and displacement currents, the relationship between the applied voltage and the current can be written as shown in Equation (6):

$$V = \frac{1}{\sigma + j\omega\varepsilon} \times l \times \frac{I}{A} \tag{6}$$

where $e^{j\omega t}$ notation has been used for a time-harmonic signal.

Dividing the permittivity by the permittivity of free space ε_0 provides the relative permittivity ε_r. The complex relative permittivity for a linear, isotropic medium can be written as shown in Equation (7):

$$\varepsilon_r = \varepsilon_r' - j\varepsilon_r'' \tag{7}$$

where ε_r' is the real part (also called the *effective relative permittivity*) and ε_r'' accounts for losses.

The conductivity σ can range in value from 10^{-6} S/m for very dry sand, rock, or fresh water ice to 10 S/m for highly saline soils. The effective relative permittivity ε_r' can range from 3 to 100 for isotropic materials, but the effective relative permittivity can assume much larger values (or even be negative) in the case of mixed and/or anisotropic media [B1.1, B1.2]. For example, a clay–loam soil with 10% water content was found to vary continuously from $\sigma = 10^{-2}$ S/m and $\varepsilon_r' = 10^4$ at 100 Hz to $\sigma = 5$ S/m and $\varepsilon_r' = 10$ at 10^{10} Hz [B1.11].

It is well known that the physical and electromagnetic properties of the earth are highly nonuniform. Consequently, the use of parameters σ and ε to describe the earth has to take into account the fact that they will be a function of spatial dimensions or will represent a composite value, which is directly affected by the nonuniformity of the sample. In rock mechanics, these differences are described by the terms "rock mass" to represent the nonuniform composite structure, and "rock material" to represent the uniform material. This distinction can also be made by differentiating between those methods of measurements that are made in situ and those that are made on rock samples in the laboratory. This distinction is also directly related to the wavelength of the radiation in the material under consideration, and the size and separation of the contact electrodes used in the measurement.

This guide does not cover electrical or electromagnetic geophysical methods [B1.10] that rely on mapping anomalies in the earth's structure, unless such information is directly related to determining the electrical properties of such materials. These geophysical techniques include magnetic tilt methods, magnetic surveys, most types of ground probing radar, and many airborne and satellite remote sensing techniques. The guide does include the methods used to provide "ground truth" for these mapping methods.

The frequency of measurement, the water content of the sample, the temperature of the sample, the pressure on the sample, and the degree of fracture of the sample will all affect measurements [B1.1]. There can be significant problems with probe contacts, both for in-situ measurements (probe impedance, conductive layers, etc.) and sample measurements (surface preparation, air gaps, etc.). In addition, these materials can be highly inhomogeneous, anisotropic, layered, and fractured so that the orientation of the electrodes should play a significant part in determining the results obtained [B1.10].

The measurements on soil samples are particularly difficult as the removal of a sample can strongly affect soil compaction and water content (particularly the water concentration profile as a function of depth) [B1.19].

In-situ measurements are commonly made from or above the earth's surface, e.g., with inserted probes, from an airborne platform, or from boreholes. In-situ measurements, where properly implemented, can avoid the problems resulting from changes in compaction and soil moisture content. An attempt shall be made to cover all of these techniques.

Given the inhomogeneous and anisotropic nature of earth mass, the derivation of reliable data from field and laboratory measurements is difficult. It is possible to find analytical solutions to certain idealized earth structures. The calculation of field results using analytical or numerical methods from a postulated earth structure is called *forward modeling*. Thus, one can derive characteristic curves to deduce ground constants. More commonly, however, automated data inversion techniques are not available as the number of unknown parameters (including their spatial distribution) is so large that least squared error minimization techniques do not converge to the correct answer [B1.18]. The mathematical techniques of numerical modeling for solving the forward problem (i.e., assuming a particular earth profile to calculate expected measurement results), and stimulated annealing and artificial neural networks for the inverse problem (i.e., determining the electrical properties of the earth from the measurements) require considerable computation time and effort. Therefore, only passing mention shall be made to numerical methods for forward modeling and data inversion for two- and three-dimensional structures.

1.2 Applications

The measurement of the electromagnetic properties of soil and rock, commonly called *ground constants*, are important for a wide variety of reasons, including:

a) Ground plane assessment for the location of antennas and assessment of the characteristics of installed antennas;
b) Estimation of the coverage area of transmitters;
c) Mapping of conductive and resistive formations to obtain geological information and locating buried objects;
d) Assessment of ore-grade quality, moisture content, salinity, etc.;
e) Propagation studies for communications links above the surface and through-rock communications systems;
f) Assessment of aquifer activity for water search, assessment of nuclear waste disposal sites, the location of dams, and rock drilling for tunnels and storage sites;
g) Measurement of surface parameters to calibrate antenna sites and remote sensing systems (including surface soil moisture content, soil salinity, aquifer location, etc).

The area of coverage of these techniques is not only frequency dependent, but also relates to the ease of use of the technique and whether it is possible to perform the measurements from an airborne platform. A very generalized surface coverage diagram for in-situ measurements is given in Figure 1.

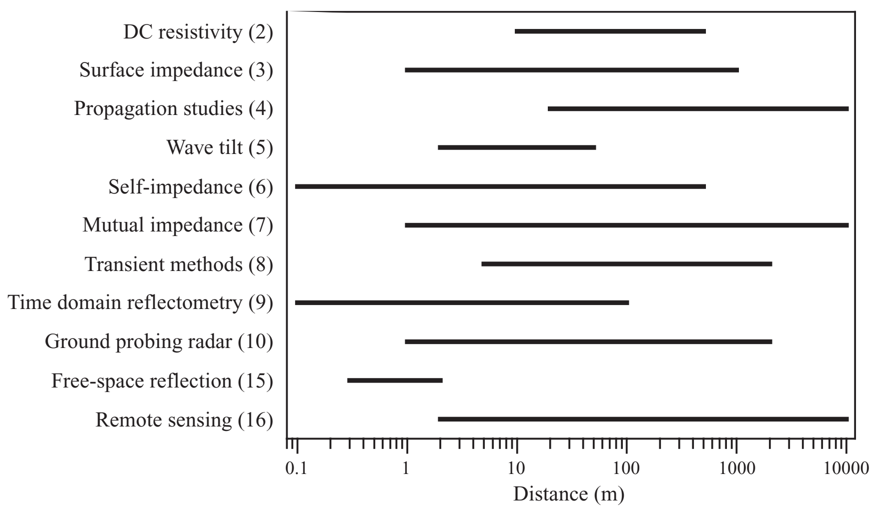

Figure 1—Approximate coverage area (linear traverse)

NOTE—The numbers in parentheses refer to the relevant clauses.

1.3 Document organization

The distinction between methods of measurement is quite blurred in many cases. However, in the interests of clarity, each different generic measurement technique shall be discussed separately. The divisions used in this guide are listed in Table 1.

As the effect of frequency is very important—not only because of the depth of electromagnetic wave penetration—but also because the electrical parameters can differ dramatically over the frequency range, Figure 2 has been included to categorize the different measurement techniques in terms of their typical frequencies of operation. Each technique is discussed in turn, with bibliography given in Annex B, as well as suggested further reading.

Table 1—Measurement method categories

In-situ measurements	Laboratory measurements
Resistivity methods (2)	Time domain reflectometry (9)
Surface impedance methods (3)	Resistivity methods (11)
Propagation studies (4)	Capacitance methods (12)
Wave tilt methods (5)	Transmission line methods (13)
Probe self-impedance (6)	Waveguide and cavity methods (14)
Mutual impedance (7)	
Transient electromagnetic methods (8)	
Time domain reflectometry (9)	
Ground probing radar (10)	
Transmission line methods (13)	
Free-space reflection (15)	
Microwave and millimeter-wave remote sensing (16)	

NOTE—The numbers in parentheses refer to the relevant clauses.

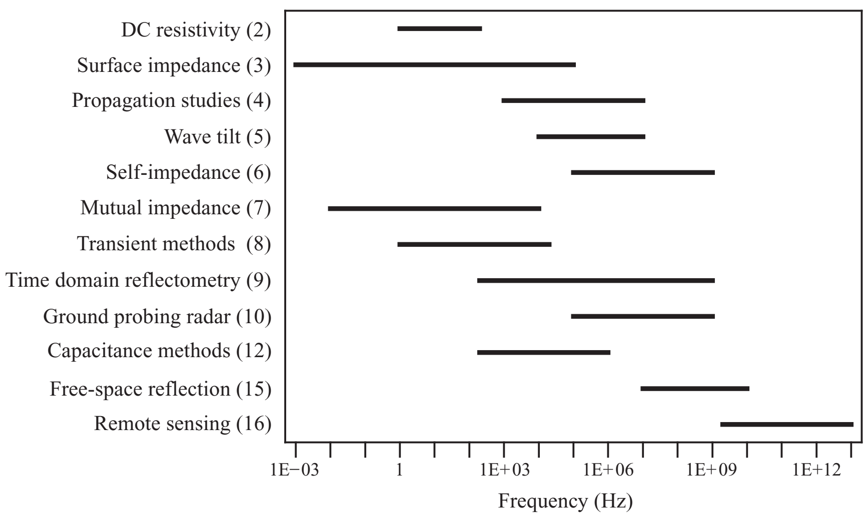

Figure 2—Frequency ranges of field methods

NOTE—The numbers in parentheses refer to the relevant clauses.

1.4 Notation

Throughout this guide, a set of standard definitions shall be used. The complex propagation constant γ for an electromagnetic wave propagating through any material is defined by Equation (8) [B1.3]:

$$\gamma = \alpha + j\beta = j\omega\sqrt{\mu(\varepsilon + \sigma/j\omega)} \tag{8}$$

where

α is the attenuation constant,

β is the phase constant,

ω is the angular frequency,

μ is the magnetic permeability of the medium,

ε is the permittivity of the medium,

σ is the conductivity of the medium,

j is the square root of –1.

The resistivity ρ of the medium is given by Equation (9):

$$\rho = \frac{1}{\sigma} \tag{9}$$

As there are losses associated with the propagation, one can attribute a finite value to the conductivity of the medium. If the medium is uniform, then the field strength of the propagating wave attenuates exponentially. The separation distance between two points along a line in the direction of propagation is designated the penetration depth (or skin depth, δ) [B1.6] if the field at one point is $1/e$ less than the field at the other. This can be defined as the reciprocal of the attenuation constant. Thus, in Equation (10) one can write:

$$\delta = \frac{1}{\alpha} \tag{10}$$

When the conduction current is much larger than the displacement current (i.e., $\sigma \gg \omega\varepsilon$), we can write an approximate expression [Equation (11)] for δ as

$$\delta \cong \frac{1}{\sqrt{\pi f \mu \sigma}} \tag{11}$$

where f is the frequency of the radiation ($f = \omega/2\pi$).

When $\sigma \approx \omega\varepsilon$, it is necessary to use the full expression for the skin depth δ derived from Equation (8) and Equation (10).

The intrinsic impedance of the medium, Z, is given by Equation (12):

$$Z = \sqrt{\frac{j\omega\mu}{\sigma + j\varepsilon\omega}} \tag{12}$$

If the conduction current dominates the displacement current in the earth, then, by using Equation (13), one can write:

$$Z \cong \sqrt{j\omega\mu\rho} \tag{13}$$

The normalized impedance Δ is the ratio of the intrinsic impedance Z divided by the impedance of free space Z_0 is given by Equation (14):

$$\Delta = \frac{Z}{Z_0} \cong \frac{Z}{120\pi} \tag{14}$$

The reflection coefficient for a plane wave in Medium 1, incident at an angle θ_i, is polarization dependent and is given by Fresnel's equations [B1.3]. Note that θ_i is measured with respect to the surface normal (Figure 3a). One can use Snell's Law [Equation (15)] to calculate the angle θ_t of the lines of constant phase in Medium 2:

$$\sin\theta_t = \sqrt{\frac{\varepsilon_{r0}}{\varepsilon_{r1}}}\sin\theta_i \tag{15}$$

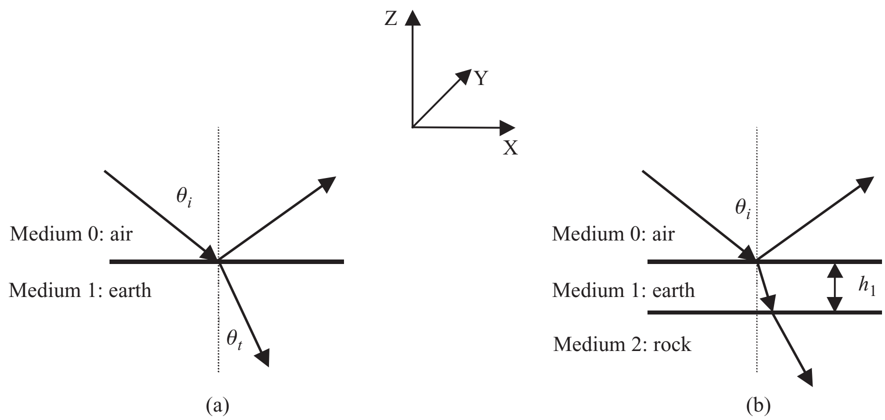

Figure 3—Schematic diagrams for electromagnetic radiation incident on the earth's surface: (a) uniform, infinitely deep earth; (b) single layer above a uniform, infinitely deep earth

In a lossy medium, ε_r is complex [Equation (7)], so θ_c will be a complex angle. From this angle, one can calculate the equation for the planes of constant amplitude and constant phase. For parallel (TM) polarization when the magnetic field vector is perpendicular to the plane of incidence, the reflection coefficient $\Gamma_{||}$ is given by Equation (16):

$$\Gamma_{||} = \frac{(Z_0 \cos\theta_i - Z_1 \cos\theta_t)}{(Z_0 \cos\theta_i + Z_1 \cos\theta_t)} \tag{16}$$

and for perpendicular (TE) polarization when the electric field is perpendicular to the plane of incidence, the reflection coefficient $\Gamma_{\perp}$ is given by Equation (17):

$$\Gamma_{\perp} = \frac{(Z_1 \cos\theta_i - Z_0 \cos\theta_t)}{(Z_1 \cos\theta_i + Z_0 \cos\theta_t)} \tag{17}$$

Note that, for any horizontally layered medium having n layers, the intrinsic impedance Z_n is given by Equation (12), i.e., Equation (18):

$$Z_n = \sqrt{\frac{j\omega\mu_n}{\sigma_n + j\varepsilon_n\omega}} \tag{18}$$

where $n = 0$, 1, and 2 are the layer numbers.

If the medium is nonuniform, it is common to assign a single parameter, the effective surface impedance, to describe interactions on the surface. Geophysicists often use apparent resistivity ρ_a to quantify the total loss measured in the medium. Thus, many geophysical techniques will yield contour maps of ρ_a and not attempt to interpret the underlying structure. In this guide, reference will be made to effective surface impedance and apparent conductivity, which are directly related to ρ_a through Equation (9), assuming that the earth is uniform and infinitely deep.

The effective impedance concept can be used to describe the reflection of electromagnetic waves from the plane surface of a nonuniform material. For example, if the earth plane is horizontally layered, it is possible to calculate the effective surface impedance for a plane wave incident from the air.

Two separate cases must be considered, TM and TE. In the general case for an angle of incidence θ_i it is convenient to define the effective impedance $\hat{Z}$ [B1.25] by Equation (19):

$$\hat{Z}_1 = Z_1 \sqrt{1 - \frac{\gamma_0^2 \cos\theta_i}{\gamma_1^2}} \tag{19}$$

where Z_1 is the intrinsic impedance of the earth defined in Equation (18), and the angle of incidence θ_i is as shown in Figure 3a.

For a uniform earth that is infinitely deep (Medium 1) the surface impedance is given by Equation (20):

$$Z_S = \hat{Z}_1 \tag{20}$$

In the TM case, for a single earth layer of depth h_1 overlying an infinite half-space (see Figure 3b), the resultant surface impedance Z_S^r is given by Equation (21) [B1.25]:

$$Z_S^r = Q_1 Z_S \tag{21}$$

where Z_S is the surface impedance of an infinitely deep earth of Medium 1 given by Equation (21), and Q_1 is given by Equation (22):

$$Q_1 = \frac{\hat{Z}_1 + \hat{Z}_2 \tanh(u_1 h_S)}{\hat{Z}_2 + \hat{Z}_1 \tanh(u_1 h_1)} \tag{22}$$

Here, $u_1 = \gamma_1 \cos\theta_1 = \sqrt{\gamma_1^2 - \gamma_0^2 \sin^2\theta_i}$, γ_0 is the complex propagation constant for free space, and γ_1 is the complex propagation constant for Medium 1; $\hat{Z}_2$ is given by Equation (19), using the electrical properties of Medium 2.

For a multilayered earth plane, one can calculate the surface impedance by calculating the intrinsic impedance of the lowest layer (i.e., assuming no reflection from a lower boundary), and use Equation (21) and Equation (22) iteratively until the upper surface of the top layer is determined. This calculation is identical to the expression used to calculate the input impedance of a multicomponent transmission line [B1.25].

In the simplest case of normal incidence, $\theta_i = 0$, the reflection coefficient $\Gamma_{||}$ is given by Equation (23):

$$\Gamma_{||} = \frac{Z_0 - Z_S}{Z_0 + Z_S} \tag{23}$$

In the TE case, the surface admittance, Y_S is given by Equation (24):

$$Y_S = Q' \hat{Y}_1 \tag{24}$$

where $\hat{Y}_1 = u_1 / j\gamma_1\omega$ and

$$Q' = \frac{\hat{Y}_2 + \hat{Y}_1 \tanh(u_1 h_1)}{\hat{Y}_1 + \hat{Y}_2 \tanh(u_1 h_1)} \tag{25}$$

When the earth electrical properties vary continuously as a function of depth (e.g., when the moisture content is varying exponentially), analytical expressions for the surface impedance and surface admittance can be derived [B1.10]. In general, the vertical gradient down to approximately one skin depth for the frequency in use has to be considered.

If the earth is anisotropic, it is possible to rotate the resistivity tensor to the direction of interest and calculate the effective surface impedance [B1.16]. This is true both for horizontally oriented anisotropy and tilted (i.e., dipping) structures [B1.22]. When the earth has a dipping, layered structure (i.e., nonhorizontal, parallel stratifications), a more complex solution is required [B1.26].

There are analytical formulas for the permittivity of materials consisting of mixtures of dielectric materials [B1.21]. Similarly, in composite materials, artificial dielectric theory can be applied to conductive particles embedded in a lossy matrix [B1.2, B1.23, B1.24]. At most frequencies, the complex permittivities of earth materials are dominated by the water content [B1.11–B1.13, B1.27]. The water distribution is often highly variable, particularly in the vertical direction. A lumped impedance RC network model, such as the Longmire–Smith (L-S) model [B1.13], allows a description of the relationship between the real and imaginary part of the permittivity. A plot of the imaginary part ε_r'' versus the real part ε_r' of the relative permittivity ε_r is referred to as a Cole–Cole plot [B1.4, B1.11]. Only recently has dispersion been incorporated into numerical methods [B1.11, B1.17, B1.20].

2. DC resistivity

2.1 Theory

DC resistivity measurements represent the most fundamental approach to determining the conductivity of in-situ materials from a surface. Two electrodes are used to make electrical contact with the surface to inject current, and the potential distribution is measured in the vicinity of the current electrodes. Despite the name, low-frequency alternating voltages and currents are used. Table 2 summarizes the common electrode arrangements and the expressions used to calculate the apparent conductivity. Note that I is the injected current, V is the voltage detected, a is the standard electrode spacing, and n is an integer. The geometry for these different electrode arrangements is illustrated in Figure 4.

Table 2—Common resistivity electrode configurations [B2.3]

Electrode arrangement	Apparent conductivity, σ_a
Wenner array	$I/2\pi Va$
Schlumberger array	$I/\pi Vna(n+1)$
Three-electrode array (pole–dipole) (Eltran array when $n=1$)	$I/2\pi Vna(n+1)$
Dipole–dipole array	$I/\pi Vna(n+1)(n+2)$
Right-angle array (Wait array)	$0.05305 \times (I/V)/a$

NOTE — I is the current, V is the voltage detected, a is the standard electrode spacing, and n is an integer.

For measurements on a semi-infinite uniform half-space (conductivity σ) using hemispherical electrodes with radius r, the resistance between one electrode R_E and a point an infinite distance away is given by Equation (26) [B2.16]:

$$R_E = \frac{1}{2\pi r\sigma} \tag{26}$$

As there can be significant difficulties in ensuring adequate contact between the electrodes and the ground, the effect of the contact is minimized by using a set of voltage electrodes and a different set of current electrodes located in the vicinity; this constitutes a four-point electrode system, and is used to map the conductivity profile of the upper parts of the earth's surface. DC current is injected into the ground at one electrode and extracted at another (the current electrodes), and two other spaced electrodes (the voltage electrodes) are used to determine the voltage for a given electrode spacing at the surface in the local area. This process usually is repeated for different electrode spacings to check for layering. Data commonly are plotted as contours of apparent resistivity covering the area surveyed [B2.3]. The right-angle array technique (or Wait array) is described in more detail in [B2.3, B2.18].

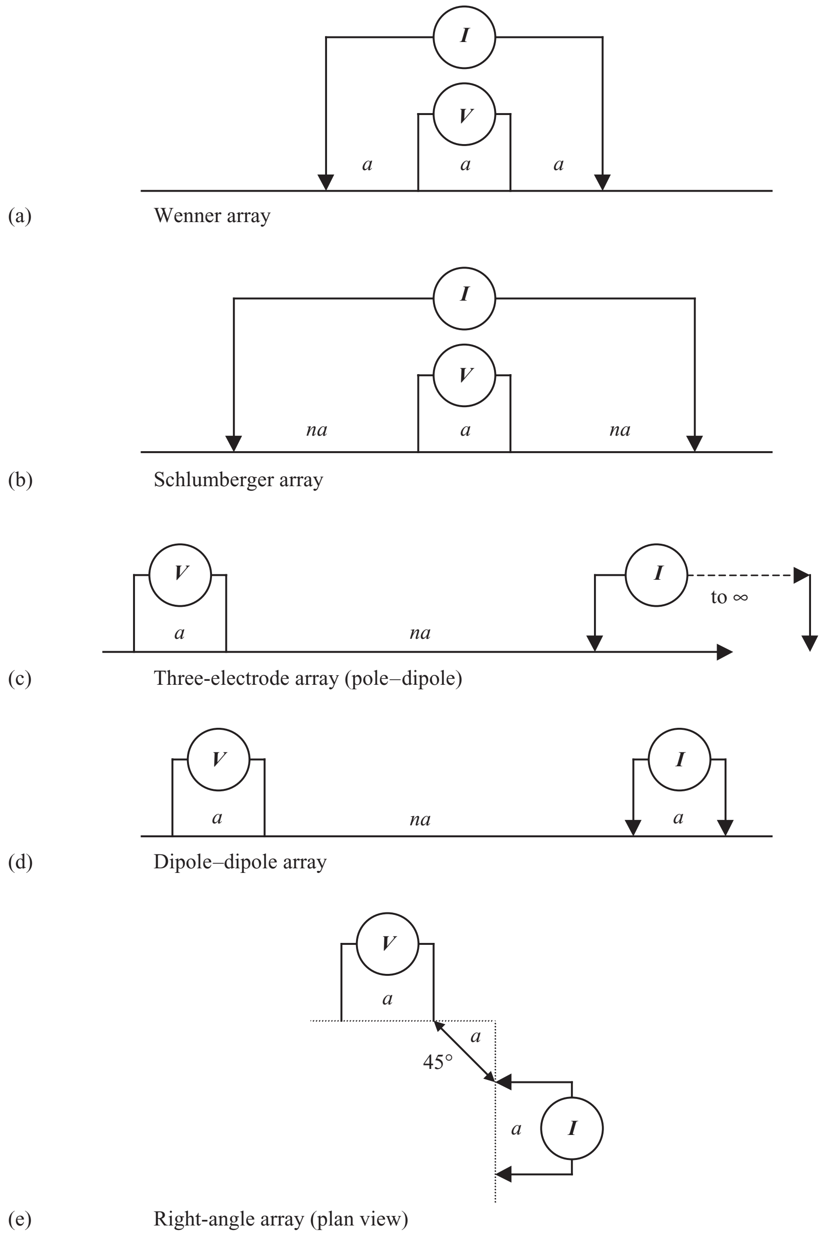

Figure 4—Common apparent resistivity arrays [B2.3, B2.5, B2.14–B2.16, B2.18]

The forward modeling problem requires the solution of Laplace's equation for the potential distribution found on the surface.

When the earth is inhomogeneous, the potential distribution is distorted. For example, current in Medium 1 flowing to Medium 2 changes direction if the conductivity is different [B2.14]. The surface potential due to horizontal bedding layers can be calculated using the method of images [B2.14] or using effective resistance calculations in an integral equation [B2.16]. Other variations in conductivity can be solved analytically. These include buried spheres, anisotropic earth materials, vertical dikes, exponentially varying conductivity, wedge-shaped anomalies, and borehole configurations [B2.3, B2.5, B2.14–B2.16, B2.18]. Numerical modeling techniques include the finite difference method [B2.9], the finite element method [B2.11], and the conjugate gradient method [B2.19].

While measurements are clearly influenced by subsurface variations in conductivity, rugged topography has a similar effect since the current tends to follow the surface. Shallow conductive layers also can result in misleading potential variations [B2.14].

When the earth is horizontally layered, the results become a function of the electrode spacing, a. Information about the conductivities of the two layers and the depth of the upper layer can be determined by multiple measurements using different spacings.

Automated inversion techniques for field survey results based on these models have been under investigation [B2.7, B2.8, B2.13, B2.19]. For example, least squared error minimization techniques combined with a forward modeling numerical technique have been investigated [B2.8, B2.11, B2.19]. For in-field use, a simple calculator-based method is available [B2.7].

2.2 Field methodology

Both dc and extremely low frequency (ELF) ac (less than 60 Hz) current sources are used [B2.14]. If the source is dc, the polarity must be reversed periodically to reduce the effect of electrolytic polarization [B2.13]. This reversal is implemented a number of times each second. While a dc source clearly yields dc resistivity, the spontaneous potentials (SP) in the earth (the basis of another method of geophysical mapping) can significantly alter the results. This bias effect can be minimized by simply noting the potential before the current source is applied, and subtracting this value from the measured results. The ac technique eliminates the SP effect, and allows the use of narrow-band amplifiers tuned to the source frequency to improve the signal-to-noise ratio. The measured resistivity is usually lower than the true dc value, and there can be interference through inductive coupling from the current supply leads.

The ac electrodes can be metallic conductors (steel, brass, aluminum, stainless steel, etc.). For dc currents, porous-pot electrodes filled with electrolyte are used [B2.5, B2.6]. The electrodes have to penetrate the ground by at least 10 cm to ensure adequate contact. The feed cables for both the current source and the potential measurements shall be insulated from the ground.

Figure 4 represents a number of the common configurations used for resistivity mapping. The larger the spacing between the electrodes, the deeper the effective area of measurement. The expressions given in Table 1 for the apparent conductivity σ_a assume a uniform earth half-space, where I and V are the injected current and measured voltage, respectively. It is clear from these expressions that the spacing between the electrodes, a, is the most important parameter in determining the volume of earth to be associated with a resulting apparent resistivity datum.

The probe resistance can cause significant problems. While the four-electrode array is independent of the probe resistance, if this is too high, then insufficient current is injected into the earth. This results in poor quality voltage measurements and an associated loss in the maximum probing depth. It is possible to model the contact points as hemispherical electrodes coated with a layer of insulation to investigate the influence of contact resistance analytically [B2.16].

In highly resistive earth, the technique can still be used effectively. In the Antarctic [B2.1], the current was provided by a 810 V voltage source and the voltmeter used had an input impedance of $10^{14}\ \Omega$.

Marine resistivity surveys have been successful in determining the resistivity of the sea floor and the layered structure beneath [B2.12]. In one example, a dipole–dipole array of nine electrodes is floated in a regularly spaced line behind a vessel. The first two inject current, and the following seven are nonpolarizing potential difference electrodes. Six voltage measurements are made, and the apparent conductivity for the n^{th} channel (σ_{an}) is calculated. These data are then inverted to give a horizontally layered interpretation that includes the resistivity of each layer and its depth.

2.3 Borehole resistivity

In-situ resistivity measurements can be made using an appropriate borehole logging tool. As with surface-based measurements, a four-electrode technique (two current and two voltage electrodes) is commonly employed [B2.5, B2.17]; however, usually only three electrodes are located in the hole. The fourth electrode is located at the surface. From the electrode configuration, one can derive an expression for the apparent resistivity [B2.5, B2.17]. The current distribution in the earth is quite broad, with the result that thin bedding planes and other fine structured features can be unrecognizable. This problem can be overcome to a certain extent through the use of a three-electrode "focused" resistivity measurement [B2.10]. The focusing is achieved through the positioning of two, quite long, guard electrodes located above and below the active electrode, and set at the same potential. The current to a surface electrode is then confined to a thin disk in the immediate vicinity of the borehole.

In one case a three-electrode array has been used, with one current electrode and two potential electrodes. The presence of water in the hole ensures good electrical contact and does not appear to affect the resistivity reading significantly [B2.2].

More recently, tomographic techniques have been used to create a two-dimensional map of the resistivity between two boreholes. For example [B2.4], one hole contains an array of current electrodes and the other an array of voltage electrodes. Current is applied to each adjacent set of current electrodes, and the voltage on all adjacent potential electrode pairs is recorded.

3. Surface impedance methods

3.1 Theory

Surface impedance measurements are made by examining the interaction of a plane electromagnetic wave with the surface of the earth.

Surface impedance measurements are used to map the conductivity profile of the upper parts of the earth's subsurface. Principal applications include the mapping of geological structure and ice depth mapping. The technique is based on three assumptions:

a) The electromagnetic waves are incident on the surface of the earth from above the surface of the earth. Consequently, the depth of investigation is limited by the skin depth of the soil for the frequency of the wave.
b) The position of measurement lies in the far field of the radiation source. This means that all calculations (i.e., forward modeling and inversion techniques) assume plane wave interactions.
c) At the frequency of interest, the air–ground interface is adequately approximated by a plane at the position of measurement.

The method was first used in the 1950s, when it was suggested that the naturally occurring low-frequency radiation around the earth could be used as the source for an electromagnetic geophysical prospecting technique. This became known as the *magnetotelluric method* [B3.2, B3.6, B3.16]. Since then, similar techniques have been used across the frequency range from 10^{-4} Hz to 20 kHz, with both naturally occurring radiation sources, which includes the magnetotelluric method (MT), the audio-magnetotelluric method (AMT) [B3.12], lightning based techniques [B3.15], and artificial sources that include controlled source audio-magnetotellurics (CSAMT) [B3.4] and VLF [B3.3]. Table 3 summarizes the main features of these techniques, including the frequency ranges of operation and source polarization. In the case of MT, the plane wave is assumed to be incident from the vertical and elliptically polarized, whereas in all other techniques the direction of propagation is almost tangential to the surface and the wave is linearly polarized.

Table 3—Principal characteristics of surface impedance methods

Method	Frequency (Hz)	Signal source	Angle of incidence	Polarization
MT	10^{-3} to 10^{2}	Ionospheric currents	Normal	Elliptical
AMT	10 to 10^{4}	Spherics	Grazing	Linear
CSAMT	1 to 10^{3}	Grounded dipole transmitter	Grazing	Linear
VLF	8×10^{3} to 25×10^{3}	Navigation beacons	Grazing	Vertical
Lightning	100 to 10^{4}	Discrete lightning	Grazing	Vertical
Radio MT	10^{5} to 10^{6}	Local transmitter	Grazing	Vertical

For transverse magnetic (TM) polarization, the surface impedance Z_S is defined by Equation (27):

$$Z_S = \frac{E_x}{H_y} \tag{27}$$

where E_x is the horizontal electric field component, and H_y is the horizontal magnetic field component measured perpendicular to E_x. The axes are defined in Figure 3. Z_S is a complex number having both amplitude and phase. The surface impedance is almost independent of the angle of incidence at frequencies when the conduction currents dominate displacement currents in the earth media. This condition typically applies to most soils for frequencies less than about 3 MHz.

The apparent resistivity ρ_a is often used as a single parameter to describe the plane earth. This is defined in Equation (28) in terms of the inverse of Equation (13); i.e.,

$$\rho_a = \frac{|Z_S|^2}{j\omega\mu} \tag{28}$$

The equations for a horizontally stratified, multilayered, anisotropic earth are given by Equation (21) and Equation (22).

When the earth has lateral changes or is anisotropic, then field scattering occurs and Z_S can no longer be interpreted in terms of a horizontally stratified earth. Abrupt lateral changes in conductivity (e.g., faults, dikes, finite sized objects, and formations) result in anomalous Z_S values. In these cases, Z_S is dependent on the plane of incidence of the incoming plane wave. In cases where the incoming wave is elliptically polarized (e.g., MT), the surface impedance is defined [Equation (29)] as a 2×2 tensor (or dyadic) [B3.18]:

$$Z = \begin{bmatrix} Z_{xx} & Z_{xy} \\ Z_{yx} & Z_{yy} \end{bmatrix} \tag{29}$$

where the tensor elements $Z_{mn} = E_m/H_n$ for $m = x, y$ and $n = x, y$.

Given the complexities of the earth's subsurface makeup, including horizontal layering, vertical dislocations, and folded structures, the forward modeling problem using analytical methods is limited to a few idealized cases [B3.9, B3.18]. Numerical modeling techniques are used to model two- and three-dimensional earth structures. In particular, the finite element method [B3.10, B3.11], integral equation methods [B3.5, B3.17, B3.19], and the finite difference time domain method [B3.8, B3.13] have been used. Automated interpretation methods for surface impedance data (referred to as *inversion*) for inhomogeneous earth structures exist [B3.7], but they are not widely used. More commonly, a one-dimensional interpretation is used [B3.20].

3.2 Field methodology

From Equation (27), it is necessary to make measurements of the complex amplitudes E_x and H_y for one-dimensional profiling, and E_x, E_y, H_x, and H_y for two-dimensional profiling. The magnetic field is commonly measured using a multiturn loop with a ferrite or laminated steel core. The electric field is commonly measured using a horizontal dipole wire antenna with conductive connections to the ground at the two ends. This configuration is similar to those used in the resistivity field survey method described in Clause 2.

Poor quality ground contact can also result in a staked antenna probe giving misleading results [B3.14, B3.21]. In ice-covered regions, this is almost impossible to accomplish. In this case, one would employ capacitive electrodes [B3.1].

It was concluded [B3.3] that

> *"Detection of E-field signals is relatively simple, employing high performance instrumentation amplifiers… in the preamplifier section. The bandwidth of 300 kHz with a gain of 10 provides stable frequency reception and the high input impedance (10^{10} ohms) produces insignificant loading on the E-field probes."*

4. Propagation studies

4.1 Theory

There are two principal methods commonly used. The first is a surface-based method where both the transmitter and the receiver are located on or close to the earth's surface. Field strength measurements [B4.4] are made as a function of separation distance. Usually the receiver is moved while the transmitter remains fixed. In the second method, at least one antenna is located underground (in a borehole, cave, or mineshaft) and the signal strength is measured, as the position of either the transmitter and/or the receiver is moved. These two methods will be discussed in turn.

The propagation of an electromagnetic wave between two antenna systems located in the earth–ionosphere waveguide (i.e., the waveguide bounded by the earth and the ionosphere) is affected by the electrical constants of the ground in between the two antennas. If the antennas are quite close together and lie close to the earth's surface, then two components of the energy arriving at the receiver have interacted with the earth: the ground-reflected ray path and the Sommerfeld wave.

If the transmitting antenna is a vertical dipole located at height h_1 over a flat earth with a surface impedance $Z_S = 120\pi\Delta$ [see Equation (14)], then the vertical field measured at a height h_2 at a horizontal range r is approximated by Equation (30) [B4.14]:

$$E_v \cong 2E_0 W \tag{30}$$

where E_0 is the electric field at unit distance, and W is given by Equation (31):

$$W = -(1/2p)(1+q_1)(1+q_2) \tag{31}$$

with

$$\begin{aligned} p &= -jkr\Delta^2/2 \\ q_1 &= jk\Delta h_1 \\ q_2 &= jk\Delta h_2 \end{aligned} \tag{32}$$

When the numerical distance $|p| > 10$, Δ is the normalized surface impedance, and W is referred to as the *Norton attenuation function*.

The q factors describe the height-gain characteristics of the propagation, and the p term, the numerical distance, describes the attenuation function in the far field of the radiating antenna. After appropriate curve matching of the experimental data, the effective electrical constants of the ground can be inferred [B4.5].

Similarly, if the transmitting antenna is a loop lying on the earth's surface, one can conduct a similar attenuation measurement to determine the surface impedance of the earth.

In the event that there are lateral changes in the surface impedance along the path, then the measurements will reveal a significant change in the impedance as a function of distance from the transmitter. This is especially evident, for example, when the path crosses a land–sea boundary [B4.7, B4.14].

If both the transmitter and the receiver are located underground, then the propagation is described by the complex propagation coefficient γ, given by Equation (8), and the attenuation is related to the conductivity and relative permittivity of the material between the transmitter and receiver.

4.2 Surface-based field methodology

Measurements of the LF attenuation as a function of distance have been made with a light aircraft flying at low altitude to minimize the height gain effect [B4.7]. The field data were normalized to the transmitter output power, and curve matching techniques were applied to determine the average conductivity over the path. Least squares curving fitting is required when the propagation is clearly over inhomogeneous paths [B4.5, B4.14]. Other conductivity maps have been generated from ground-based surveys of commercial radio transmitters [B4.5].

The complex permittivity of Antarctic ice was determined by measuring the phase velocity of a VLF signal [B4.11]. Glacial interiors and the surface of planetary bodies have been investigated by curve fitting the field strength versus distance measurements at a number of RF frequencies [B4.6].

These surface-based measurements are influenced significantly by the surface topography [B4.1, B4.16] and by surface features such as vegetation [B4.15] and buildings [B4.8].

4.3 Borehole and other underground applications

The measurement of path attenuation along a borehole has been used to deduce the electrical properties of the surrounding earth [B4.2]. In this case, a small transmitter was lowered down the hole, and the field strength at the surface was measured as a function of transmitter depth.

Borehole tomography uses two boreholes, one for the transmitter and the other for the receiver [B4.10]. The attenuation across the path is determined as a function of depth for both the transmitter and receiver. A two-dimensional (2D) image of the attenuation in the rock between the two boreholes can then be resolved using standard tomographic techniques [B4.10].

Durkin [B4.3] used magnetic loops, operating in the frequency range 630–3030 Hz, for probing underground coal seams in more than 20 different mines. The input signal was a square wave and the data were processed by Fourier transform for final analysis and interpretation. It was found that the conductivity of the material decreased with depth.

This technique has been broadened for use in underground mines to map the attenuation of a radio signal through solid rock lying between two horizontal mine roadways. The technique (radio imaging, RIM) allows the generation of 2D images of attenuation using tomographic techniques [B4.12, B4.13].

The relationship between the attenuation and the electrical constants of the earth is not straightforward, and so the technique is used to locate inhomogeneities in the earth rather than to estimate conductivity and permittivity values. Various numerical modeling techniques (integral method, FDM) have been used for forward modeling through geological structures [B4.9].

5. Wave tilt methods

5.1 Theory

When the radiation from a distant radio transmitter is vertically polarized, and incident on the earth's surface at grazing incidence, there are two components of the electric field, a vertical component E_z (i.e., perpendicular to the earth's surface) and a horizontal component E_x (i.e., parallel to the earth's surface). These two field components are commonly out of phase and the electric field vector is tilted forward [B5.1]. In the horizontally polarized case, the magnetic field is tilted.

Wait [B5.6] and King [B5.3] have published expressions [Equation (33) and Equation (34)] for the TM (vertical polarization) wave tilt W_e and TE (horizontal polarization) W_m wave tilt in terms of the normalized surface impedance Δ, i.e., the surface impedance divided by the free-space impedance ($120\pi\ \Omega$).

$$W_e = \frac{E_y}{E_x} = \frac{\Delta(\theta)}{\sin\theta_i} \tag{33}$$

and

$$W_m = \frac{H_x}{H_y} = \frac{\delta(\theta)}{\sin\theta_i} \tag{34}$$

where θ_i is the angle of incidence measured with respect to the surface normal (see Figure 3) and $\delta(\theta)$ is the normalized surface admittance.

As both $\Delta(\theta)$ and $\delta(\theta)$ are complex, so then W_e and W_m are complex.

In most cases, the TM propagation mode suffers less path attenuation, and so most fieldwork has been performed by measuring the electric field wave tilt, W_e, with a vertically polarized radiation source.

5.2 Measurement techniques

The measurement of the two field components on the earth's surface can be undertaken by two orthogonal dipoles in the TM case [B5.2], and by two orthogonal loop antennas for the TE case. In most cases, the dual antenna combination is manually rotated about a horizontal axis perpendicular to the plane of incidence. As the magnitude of the wave tilt is commonly very small, there are significant instrumental problems in determining this very small, horizontal field component in the presence of the very strong vertical electric field [B5.5].

There are significant difficulties associated with making these measurements. These include:

a) The changing antenna impedance due to earth coupling
b) The effect of the measurement electronics (including cables) on the measurement
c) The effect of the operator on the measurements
d) The finite size of the antennas
e) Antenna alignment errors

For these reasons, the ground-based technique has not found favor in ground survey work.

It has been suggested that an airborne wave tilt measurement might solve some of these problems [B5.4]. However, in order to minimize the effects of aircraft vibration and other misalignment problems, the phase quadrature of the horizontal electric field is measured in order to minimize coupling of the horizontal antenna into the much stronger vertical electric field. If only the phase-quadrature component is measured, it is impossible to determine the complex permittivity of the ground, and the technique becomes one in which only anomalies in the field can be detected. In addition, the rapid variation in the electric field wave tilt as a function of altitude also has ramifications on the overall accuracy of the technique. The airborne wave tilt technique has not been investigated experimentally to our knowledge.

6. Probe impedance (self-impedance) methods

6.1 Theory

It is possible to determine the electrical properties of the earth by measuring the input impedance of a probe located either in air close to the surface or embedded in the earth. A number of probe configurations can be used, including a dipole and a monopole (either insulated or bare) [B6.1, B6.7, B6.9–B6.12], and various configurations of parallel conductor transmission lines.

Above the surface, both the height of the dipole and the electrical characteristics of the earth [B6.1] affect the input impedance of horizontal electric and vertical magnetic dipoles. This strategy has been used by measuring the input impedance of a horizontal, near resonant, electric dipole located in air immediately (i.e., $h \leq \lambda/10$) above the earth's surface [B6.10].

There are several methods for measuring the electrical properties of the earth in situ that make use of probes embedded in the ground. These include both antennas and transmission lines. Figure 5 shows three typical arrangements. In all cases, the input impedance, Z, of the probe is measured at a single frequency or over a range of frequencies with a device such as a vector network analyzer or impedance bridge, and the electrical parameters of the surrounding medium (σ, ε_r) are obtained by a mathematical inversion process. In most cases, the probe is first calibrated by making measurements in a medium with known electrical properties (e.g., air).

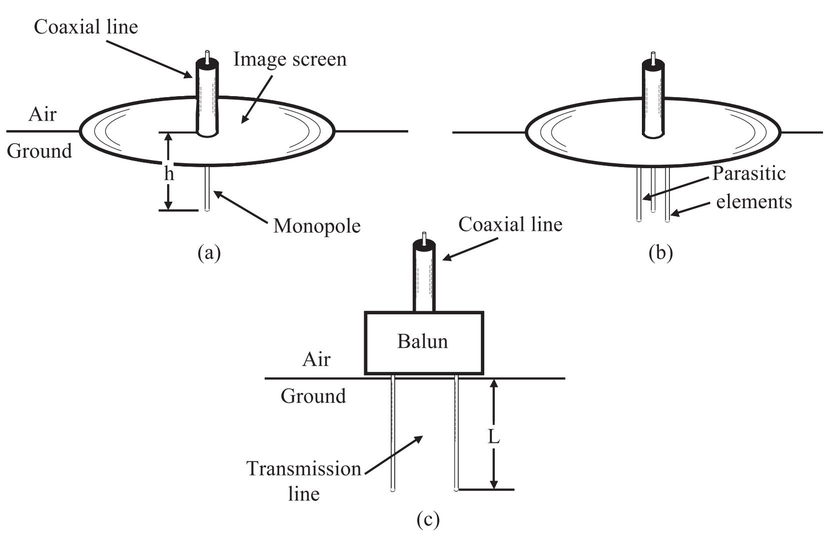

Figure 5—Probes for the in-situ measurement of the electrical properties of the ground: (a) monopole probe with ground plane (image screen); (b) monopole probe with parasitic elements; (c) parallel-wire transmission line probe

In the inversion, an electrically homogeneous medium is assumed, so when inhomogeneities do exist, the procedure produces a spatial "average" of the electrical properties of the medium surrounding the probe. These methods are generally used at frequencies (HF and above) where electrochemical effects at the metal/soil boundaries are insignificant. However, care must be taken when the probes are inserted into the ground to avoid creating air gaps at these boundaries.

The simplest impedance probe is the monopole antenna with a circular ground plane (i.e., an image screen) as shown in Figure 5a. Here, a metal rod is inserted vertically into the ground, and a horizontal, metal image screen is placed on the surface of the ground over the rod. The rod is fed through the image screen by a coaxial transmission line. The input impedance/admittance of the monopole is measured and used to infer the electrical properties of the surrounding medium. When the electrical length of the monopole is very small, $|kh| \ll 1$, the antenna behaves as a lossy capacitor, and the relationship between the input admittance and the electrical properties [Equation (35)] is fairly simple [B6.7]:

$$Y = G + jB = j\omega C_{\mathrm{air}}\left(\varepsilon_r - \frac{j\sigma}{\omega\varepsilon_0}\right) \tag{35}$$

Here, C_{air}, the capacitance of the antenna in air is a constant, which can be determined from a calibration measurement. For electrically longer monopoles, the inversion procedure is more complex [B6.7].

One inversion procedure is based on a rational fraction approximation to the impedance [B6.16]. When the order of the rational fraction is three, the normalized impedance is approximated by Equation (36):

$$\begin{aligned} Z_n &= \frac{kh}{k_0 h} Z \\ &\approx -j\left(\frac{h}{cC_{\mathrm{air}}}\right)\frac{1}{kh}\left[\frac{1 + jb_1(kh) + b_2(kh)^2}{1 + jb_1(kh) + a_2(kh)^2}\right] \end{aligned} \tag{36}$$

where

$$k_0 = \omega / c \tag{37}$$

and

$$k = \beta - j\alpha = k_0\sqrt{\varepsilon_r - j\sigma/\omega\varepsilon_0} \tag{38}$$

The four real constants $(C_{\mathrm{air}}, a_2, b_1, b_2)$ in Equation (36) are determined from calibration measurements made with the probe in a material with known electrical properties. With the probe in an unknown material, the impedance Z is measured. This impedance is inserted into Equation (36), which is then rearranged to form a polynomial of fourth degree in kh. The polynomial is solved for kh, and ε_r and σ are determined from Equation (38) [B6.16]. This procedure is limited by the approximation to the impedance, which is accurate for monopoles of electrical length $|kh| \le \pi/2$. For electrically longer monopoles, a more general inversion procedure is available [B6.15]. The monopole antenna radiates energy into the surrounding medium where it is attenuated by dissipation. The distance from the monopole to any object that can reflect this energy, such as the edges of the image screen, has to be sufficiently large so that these reflections are negligible when they return to the monopole. When this requirement cannot be met, the structure shown in Figure 5b can be used [B6.17]. Here, two closely spaced parasitic elements are placed at the sides of the monopole. These elements reduce the radiation from the monopole and, therefore, the reflected energy from nearby objects. The calibration procedure is similar to that used with the monopole antenna.

The method shown in Figure 5c uses a section of parallel-wire transmission line of length L inserted vertically into the ground as the probe [B6.2, B6.8]. A balun should be used to connect this probe to conventional measurement apparatus with a coaxial input, such as a network analyzer. Thus, the characteristics of the balun must be taken into account when obtaining the input impedance of the probe. A simple probe adaptor can be used for frequencies below 30 MHz [B6.8]. In this case, the impedance transformation of the adaptor must be taken into account through calibration measurements. The effects of a balun (or probe adaptors in the absence of a balun) can be determined by measuring the input impedance under open-circuit and short-circuit conditions.

The input admittance of the transmission line is given by Equation (39):

$$\begin{aligned} Y &= j\frac{Y_0}{k_0 L}[kL\tan(kL)] \\ &= j\omega\frac{C_0 L}{(k_0 L)^2}[kL\tan(kL)] \end{aligned} \tag{39}$$

where Y_0 and C_0 are the characteristic admittance and capacitance per unit length, respectively, of the air-filled line. When the electrical length of the transmission line is very small, $|kL| \ll 1$, it behaves as a lossy capacitor, and the relationship between the input admittance and the electrical properties [Equation (40)] is fairly simple [B6.7]:

$$Y = G + jB = j\omega C_0 L\left(\varepsilon_r - \frac{j\sigma}{\omega\varepsilon_0}\right) \tag{40}$$

For longer lengths, the inversion procedure consists of inserting the measured value of Y into Equation (39), solving for kL, then determining ε_r and σ [Equation (38)] [B6.14].

An alternative transmission line technique requires the measurement of the complex impedance of a set of parallel wires inserted into the ground. The method, referred to as the open-wire line (OWL) technique, is used to measure the moisture content distribution in the upper layers of soil [B6.6, B6.8]. An electrically short parallel wire transmission line in a low-loss dielectric has a relative permittivity ε_r given by Equation (41):

$$\varepsilon_r = \frac{C_{\text{ground}}}{C_{\text{air}}} \tag{41}$$

where C_{ground} is the shunt capacitance of the transmission line in soil, and C_{air} is the capacitance in air. The conductivity of the ground is related to the dissipation factor D by Equation (42):

$$\sigma \cong \omega\varepsilon_0\varepsilon_r D \tag{42}$$

6.2 Measurement techniques

The most critical part of all probe impedance measurements is the presence of, and variations in, the air gap between the probe and the earth. For an antenna located above the earth's surface, the impedance is very much height dependent [B6.2, B6.18]. For this reason, the antenna input impedance versus height can be used to infer σ and ε_r from a set of parametric curves produced by forward modeling.

The self-impedance method requires a measurement of the input impedance of the antenna. This can be achieved by balancing a RF bridge [B6.10], although the spacing of the antenna is critical to the measurement. For this reason, measurements are usually made at a number of heights above the surface of the earth. The useful range for variation of the height of a balanced horizontal dipole is between $\lambda/1000$ and $\lambda/10$ [B6.2].

A limitation of using parasitic elements or a parallel wire transmission line is that a constant spacing has to be maintained as the conductors are "driven" into the ground. This can be difficult when the soil is hard or contains rocks, but the use of a jig can help maintain a parallel alignment.

Field use of the OWL technique was made in the frequency range 2–30 Hz for the assessment of over 50 antenna sites [B6.3–B6.5]. The probe assembly (two parallel stainless steel, brass, or aluminum rods) allowed changing the rod spacing between 5 and 10 cm and depth from 5 to 100 cm. For every site location tested, the skin depth was computed using Equation (11) and the length of the probe was adjusted to ensure that the reactance remained capacitive.

6.3 Borehole applications

Sometimes the electrical properties are required at deeper depths. For these cases, the probe generally cannot be embedded directly in the ground, but must be placed in a borehole [B6.7, B6.11, B6.19].

Figure 6 shows a typical configuration; the borehole is vertical, and the probe is a dipole concentric with the borehole. The problem is now one involving two materials: the material in the borehole (σ_b, ε_{rb}), which is generally a fluid, and the surrounding ground (σ_g, ε_{rg}). Any scheme for inversion has to be able to remove the effect of the borehole.

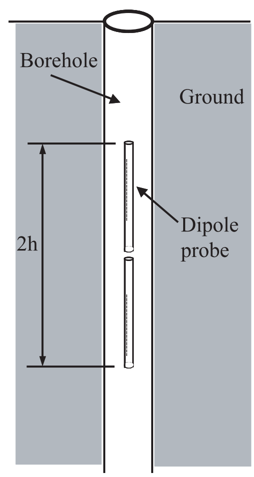

Figure 6—Dipole probe in a borehole

When the electrical length of the dipole is very small, $|k_b h| \ll 1$ and $|k_g h| \ll 1$, the input admittance of the dipole is approximately a series connection of two admittances (lossy capacitors) [Equation (43)]; one, Y_b, depends on the electrical parameters of the borehole [Equation (44)], and the other, Y_g, depends on the electrical properties of the ground [Equation (45)] [B6.7]:

$$Y \approx \frac{Y_b Y_g}{(Y_b + Y_g)} \tag{43}$$

with

$$Y_b = j\omega C_{0b}\left(\varepsilon_{rb} - \frac{j\sigma_b}{\omega\varepsilon_0}\right) \tag{44}$$

and

$$Y_g = j\omega C_{0g}\left(\varepsilon_{rg} - \frac{j\sigma_g}{\omega\varepsilon_0}\right) \tag{45}$$

and where C_{0b} and C_{0g} are the capacitances associated with the borehole material and the surrounding ground, respectively.

When there is not a large difference between the electrical properties of the material in the borehole and the surrounding earth, Equation (41) and Equation (42) can be inverted to obtain the electrical properties of the ground. However, in some situations, such as when $\varepsilon_{rg} \gg \varepsilon_{rb}$, we have $|Y_g| \gg |Y_b|$, and the admittance of the dipole is insensitive to the electrical properties of the ground, Equation (46) applies:

$$Y \approx Y_b \tag{46}$$

An electrically short, insulated dipole probe has been used in a borehole in Antarctic ice, and its input impedance measured as a function of depth. Results were correlated with ice temperature and pressure [B6.13]. Measurements were made in the frequency range 300 Hz–20 kHz, and a least squares minimization optimization method was used to deduce the complex permittivity of the ice.

A similar technique, but with the ends of the dipole exposed to make electrical contact with the surroundings, has been used in drill holes [B6.19].

7. Mutual impedance methods

7.1 Theory

In mutual impedance methods, two antennas (one at the transmitter and one at the receiver) are located in close proximity to the earth's surface and in the electrical near field with respect to each other. The separation distance between the two antennas remains fixed as the unit is moved across the earth's surface at constant height. The most common antennas used are loops for both transmitter and receiver [B7.6, B7.12, B7.14]. The signal from the transmitter is commonly at a single frequency.

For clarity, Clause 7 deals only with small loop sources and continuous wave (CW) excitation. Clause 8 deals with large loop sources (e.g., staked dipole) and pulsed sources.

A variety of loop orientations and loop separations are employed (see Figure 7). In the limit, the centers of the loops are colocated, but the loops lie in orthogonal planes. This is the principle used in hand-held metal detectors for locating shallow metal objects at shallow depths [B7.4], and also in towed bird technologies in which the transmitter and receiver loops are located in a single unit (called a "bird") suspended from a helicopter or light aircraft.

As the receiving loop lies in the near field of the transmitter, one can describe the interaction as mutual coupling between the loops. The proximity of the earth affects this coupling from that found when both antennas are located in free space, and lateral changes in the earth's conductivity induce secondary magnetic fields, which are detected by the receiver.

There are four loop configurations commonly used. One can describe these configurations [B7.14] as System 1 (horizontal loop transmitter and coplanar horizontal loop receiver), System 2 (vertical loop transmitter and coaxial vertical loop receiver), System 3 (horizontal loop transmitter and vertical loop receiver), and System 4 (vertical loop transmitter and coplanar vertical loop receiver). These are shown in Figure 7.

One can apply the quasi-static assumption if the center-to-center spacing between the two loops, r, is very much less than a free-space wavelength. If Z_0 is the mutual impedance describing the coupling between the antennas in free space, then the coupling Z between the antennas with a uniform earth half-space is given by Equation (47), Equation (48), Equation (49), and Equation (50) [B7.7, B7.14]:

System 1:

$$\frac{Z}{Z_0} = \frac{2}{(\gamma r)^2}\left[9 - \frac{9 + 9\gamma r + 4\gamma r^2 + \gamma r^3}{e^{\gamma r}}\right] \tag{47}$$

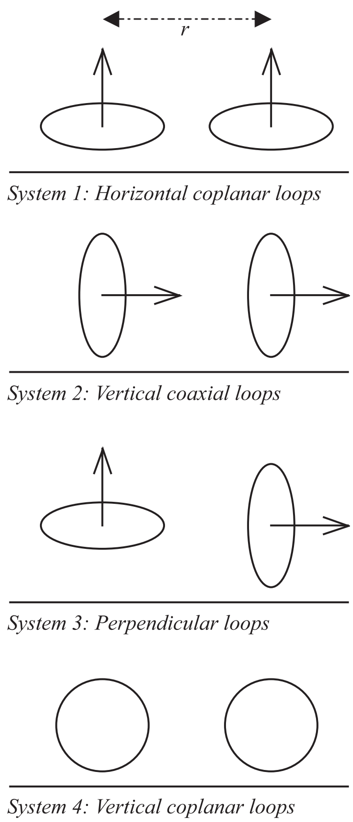

Figure 7—Induction sounding-loop configurations

System 2:

$$\frac{Z}{Z_0} = -\frac{1}{2}[(\gamma r)^2(I_1K_1 - I_0K_0) + 4\gamma r(I_1K_0 - I_0K_1) + 16I_1K_1] \tag{48}$$

where I_0, I_1, K_0, and K_1 are the modified Bessel functions with argument $\gamma r/2$.

System 3:

$$\frac{Z}{Z_0} = \frac{e^{-\gamma r}}{(\gamma r)^2}[12 + 12\gamma r + 5(\gamma r)^2 + (\gamma r)^3] + 2 - \frac{12}{(\gamma r)^2} \tag{49}$$

System 4:

$$\frac{Z}{Z_0} = 2\left\{\frac{e^{-\gamma r}}{(\gamma r)^2}\left[3 + 3\gamma r + (\gamma r)^2\right] + 1 - \frac{3}{(\gamma r)^2}\right\} \tag{50}$$

where γ is the propagation coefficient defined by Equation (8).

Additional analytical expressions can be developed for the mutual coupling when the ground is horizontally layered, in the vicinity of a buried conductive sphere, a vertical conductive sheet, and an inclined conductive sheet [B7.6, B7.12, B7.14].

In the case of a multilayered earth, when the transmitter dipole is vertical, the equations to determine the effective impedance of the earth require an iterative calculation of the admittance of successive layers. This follows the transmission line analogy for a layered earth given in Clause 2 [B7.14].

A radio frequency, three-coil mapping system has been developed for land vehicle use [B7.1, B7.13]. Termed the Laboratory for Advanced Subsurface Imaging (LASI) high-frequency ellipticity system, the system operates in the frequency range 31 kHz to 32 MHz, and employs three mutually orthogonal air-core receiver coils, and tuned transmitter coils. While used for object location, the unit also provides a mapping mode in which apparent resistivity values are calculated.

7.2 Measurement techniques

Multiturn, air-cored wire loops are commonly used for transmitter antennas, and multiturn, ferrite cored wire loops are commonly used for receiver antennas in airborne systems. Air-core loops are common for both transmitter and receiver antennas in surface-based measurements. This allows one to approximate the antenna as electrically small (i.e., as a magnetic dipole). There are three different measurement strategies [B7.15]:

a) measurement of the amplitude and phase of the received signal,
b) measurements of the in-phase and quadrature-phase components of the received signal,
c) measurement of the tilt angle of the received signal.

In the first two methods, a phase reference from the transmitter is required.

From a practical perspective, one must ensure that the spacing and orientation of the two loops remains constant. This can be achieved by mounting both antennas on the same frame, e.g., on a rigid boom [B7.9, B7.11] or on a towed sensor system [B7.3, B7.8], or by using distance-measuring equipment to maintain a constant separation [B7.11]. The frequencies used typically lie in the range 95 Hz to 25 kHz, depending on the depth of exploration required [B7.7].

The determination of the effective conductivity can be made as a direct readout from the instrument. The accuracy of the measurement is affected by loop alignment, local electromagnetic noise, and high local ground conductivity [B7.11]. Data interpretation for a multilayer, planar earth plane can be achieved from sets of standard curves [B7.11].

7.3 Borehole methods

The measurement of mutual coupling in boreholes is commonly referred to as *induction logging* [B7.2]. In a common configuration [B7.6], the transmitter and receiver loops are located on the same axis (the axis of the borehole), and separated by a grounded ring. At low frequencies, the apparent conductivity is given by Equation (51):

$$\sigma_a = \frac{I}{KV} \tag{51}$$

where K is a factor that depends on the geometrical arrangement, V is the measured voltage, and I is the current in the transmitter loop. Clearly, Equation (51) illustrates that the conductivity is directly proportional to the rock conductivity [B7.11].

In an alternative borehole method [B7.16], the transmitter loop is located on the surface of the earth, and measurements of the field are made along the length of the borehole.

One difficulty with data interpretation from induction borehole logging is the effect of water in the borehole [B7.5].

8. Transient electromagnetic methods

8.1 Theory

Two different methods are employed for transient electromagnetic (TEM) sounding. One technique uses a fixed transmitter (usually laid out as a loop or dipole on the surface of the earth), and the other uses a moving transmitter (usually a small loop mounted on an aircraft or other moving vehicle). In both cases, the transmitter is pulsed with a relatively high current pulse, and the received transient waveform is recorded and analyzed. All of the induction sounding loop configurations (see Figure 7) have been used in TEM sounding.

The transmitter provides a fast turn on or off, high-current pulse. The current is cycled between forward and reverse polarity through the coil. The receiver is synchronized with the transmitter. Some commercial techniques use the on-time characteristics and others use the off-time characteristics [B8.5, B8.7]. A more recent variation of this technique is the inductive source resistivity method, which uses an ungrounded transmitter and noncontact electrodes for signal detection [B8.4]. While initially this method failed to yield absolute resistivity values, it is no longer a limitation [B8.3, B8.4]. For a horizontally layered earth plane, the conductivity profile σ measured as a function of the reference depth h is given by Equation (52):

$$\sigma = \frac{1}{\mu}\frac{d^2 t}{dh^2} \tag{52}$$

For more complex earth structures, the calculation of the apparent conductivity from such measurements is quite difficult analytically [B8.3, B8.4, B8.6–B8.8, B8.11]. Data interpretation of the apparent conductivity, determined as a function of frequency, is often based on sets of master parametric curves that differ for each loop configuration. One approach with such curves is to normalize the data to the conductivity of the top layer [B8.7, B8.8]. More recently, a highly effective conjugate-gradient method of data inversion has been developed [B8.10].

8.2 Field procedures

The ground-based transmitter is normally supplied current of approximately 5 A although the higher-powered units can achieve 50 A [B8.6]. A number of different transmitter pulse techniques are used. They include (see Figure 8)

- — Pure impulses (alternating positive and negative square pulses with a zero resting position between each pulse).
- — Half-sinusoidal pulses (alternating positive and negative sinusoids with a zero resting position between each pulse).
- — Linear impulse ramps (alternating positive and negative trapezoidal pulses with a zero resting position between each pulse).
- — Linear ramps (triangular wave form).

The field strength is then monitored for periods of up to several hundred milliseconds, usually in the form of a set of predefined windows [B8.5]. The field at each time-step window is averaged; up to 32 windows are used. The window arrangements are different for each commercially available system and are used to resolve different subsurface features.

In airborne applications, both the transmitter and receiver are located on or towed behind the aircraft. Most commercial systems run at audio frequencies [B8.1].

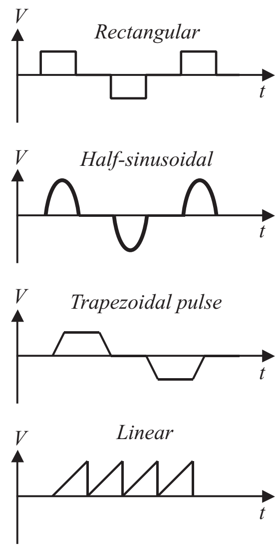

Figure 8—TEM source waveforms

8.3 Borehole transient electromagnetic measurements

The current source for a TEM system can be located in a borehole, and the surface of the earth can be surveyed using a staked dipole receiving system [B8.9]. From these measurements, one can apply a simple analytical formula to calculate the apparent conductivity of the equivalent half-space [B8.9]. Also under consideration is the location of a fixed receiver in a borehole and a moving transmitter located on the surface [B8.2]. This clearly allows a much higher transmitter power to be used.

9. Time domain reflectometry

9.1 Theory

A pulse of EM energy launched at one end of a parallel transmission line located in a lossy material will have a complex propagation coefficient γ. If the medium around the transmission line and at the termination of the line changes, the pulse will be reflected at each discontinuity. Time domain reflectometry (TDR) requires an analysis of the propagation along the two-wire transmission line of finite length where one end located in the ground is open circuited and the other end on the surface is connected to a balanced source. The time of flight of the wave propagated along the line is directly related to the effective permittivity ε_r' of the medium in which the line is inserted. The on transient and the off transient of a square wave can be analyzed if the line is very short, or if the attenuation along the line is very high. The same result can be achieved by making measurements in the frequency domain and then transforming the data into the time domain. The decrease in amplitude for successive reflections provides the data for calculating σ. The resulting electrical properties inferred are the effective values over the frequency band of the pulse averaged over the length of the probe. It is very important to note that this is a wide-band technique, and the conductivity σ and permittivity ε often show a significant variation with frequency.

The reflection coefficient at any discontinuity along the line results in a signal echo that can be interpreted at the source. The reflection coefficient is given in terms of the characteristic impedance of the transmission line, which is directly related to the complex propagation coefficient in the medium

[Equation (8)]. The velocity of the pulse is simply determined by measuring the difference between the time of the transmitted pulse and the arrival time of the reflected pulse [B9.5]. From these two measurements, both the loss along the line and the change in impedance at each discontinuity can be determined.

The technique has been used in measuring the electrical properties of ice [B9.5] and soil [B9.3]. Since the effective relative permittivity $(\varepsilon_r - 1)$ is linearly related to moisture content (by volume) [B9.4], commercial soil moisture content meters have been developed using TDR technology.

The TDR technique has also been suggested for plane wave propagation through the measurement of surface impedance over a broad band of frequencies [B9.2]. By sweeping the frequency over a broad range, the surface impedance measurement as a function of frequency can be transformed into the time domain, resulting in a plot of impedance versus time of flight. From this information, the propagation velocity can be determined from the first significant reflection layer in a horizontally stratified earth plane providing that the upper layer is not too lossy. The measured phase velocity in the upper layer is related to the complex permittivity of this layer.

9.2 Measurement techniques

A number of transmission line configurations have been investigated, including a coaxial line, two parallel rods, parallel plates, and quadrant arcs [B9.5]. The characteristic impedance Z_0 of each of these transmission lines is different, but each is modified by the presence of the dielectric material. If the material is low loss (e.g., ice), the transmission line impedance Z is given by Equation (53):

$$Z = \frac{Z_0}{\sqrt{\varepsilon_r}} \tag{53}$$

and the reflection coefficient Γ is given by Equation (54):

$$\Gamma = \frac{Z - Z_0}{Z + Z_0} \tag{54}$$

There are significant problems with the technique because the process of inserting the wires disrupts the medium. In inflexible materials, there may be places along the transmission line where there is an air gap and the propagation constant is affected significantly [B9.5]. In highly conductive materials, the attenuation and dispersion are very large, so the distance of measurement is correspondingly small.

TDR measurements have been made on sea ice in the laboratory and also in the field [B9.5] and, with an appropriate change in orientation of the sample with respect to the transmission line, the anisotropy can be determined. In the field, a ladder array of parallel transmission lines was used to determine the change in electrical parameters with depth. These TDR measurements on ice used a high-speed pulse generator and a sampling system that transformed the high frequency into a low frequency with a sharp rise time. An oscilloscope was used to record the output transient voltage.

Recently, TDR has been used to measure the modal structure on a long wire antenna lying on the surface of the earth [B9.1]. Results covering the frequency range 10 MHz–10 GHz can be interpreted in terms of a horizontally stratified medium.

Loose material such as soil can be packed into a coaxial transmission line and the dielectric properties measured at UHF frequencies using an impedance bridge [B9.1, B9.2]. Differences in moisture content and soil compaction can cause the results to differ significantly from the in-situ measurements of the same soil [B9.6].

10. Ground probing radar

10.1 Theory

Ground probing radars (GPR), like other forms of radar operating in air, use a high-frequency electromagnetic pulse launched into the medium. A receiver system records pulses reflected from propagation discontinuities along the radar range. As the perceived target depth is affected linearly by $1/\sqrt{\varepsilon_r}$, some estimate of ε_r is required to interpret the data. The maximum range of the radar is determined by the attenuation along the path (a function of the ground conductivity σ), the magnitude of the reflection from the target, and the noise level at the receiver. In the case of ground-probing radars operating over earth planes that have significant loss, the range is generally quite limited and very much frequency dependent. A common use of GPR is to detect subsurface anomalies in conductivity and permittivity, and in these applications no determination of the electrical constants of the earth or of the targets is made.

Three different radar systems are used for earth probing purposes:

a) Surface-based radars for soil and rock mapping and locating buried objects [B10.4]
b) Ice radars [B10.2]
c) Airborne and satellite based radars [B10.1].

Surface-based radars have only recently attained commercial prominence as a useful tool for pipe and tunnel detection, in structural engineering, and pre-mining assessment. Ice radar has been the preferred technique for ice depth mapping for many years. Radar altimeters on aircraft were forced to use higher frequencies to avoid receiving echoes from ice layers below the air–ice interface. Airborne radars were developed in the 1970s for soil moisture assessment [B10.1], and since then they have been found to have far broader applications.

The finite-difference time-domain (FDTD) numerical method of forward modeling has proved very useful in both the optimization of radar pulse design [B10.5], and the prediction of structures from radar measurements [B10.3].

The identification of the relative permittivity–depth profile can be undertaken using a layer stripping technique [B10.6].

10.2 Measurement techniques

GPR systems are normally bistatic, i.e., the transmitting antenna is separated from the receiving antenna. The two antennas are mounted on a single movable platform at a fixed separation distance from each other and the ground. The frequency range of operation is a compromise between target resolution and the depth of penetration of the radar pulse, but commonly lies in the range of 30 MHz to 2 GHz. In most cases, GPR is used for the location and identification of buried objects and other inhomogeneities common in geophysical prospecting. The measurement of ground constants is not a normal outcome, except during radar calibration.

In most cases, the beamwidths of both the transmitting and receiving antennas are quite large so that each discrete object traversed will result in an image with a characteristic bow-wave pattern. To complicate matters, multiple reflections between the object and the surface result in a large number of false echoes in the image. False echoes also result from nearby above-ground targets (power transmission lines, trees, etc.). If the number of scattering objects is very high, then significant image processing is required to permit interpretation [B10.7].

Given the significant frequency dependence of the conductivity and permittivity of rock and soil samples, the laboratory measurement of these parameters at these frequencies is of considerable interest [B10.8].

11. Laboratory resistivity methods

11.1 Theory

In a method similar to the field-based resistivity technique (Clause 2), resistivity measurements can be made on laboratory rock samples [B11.3]. One convenient shape for such tests is a rock core extracted from a borehole following diamond drilling. A four-electrode technique is used, where the ends of the cylinder of area A are covered with metal caps and used as the current electrodes (Figure 9). The potential difference is measured on the cylinder, using wire rings separated by a distance L and using a high-input impedance voltmeter.

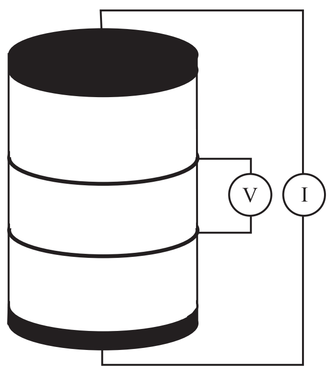

Figure 9—Electrode configuration for resistivity measurements made on rock core samples

The apparent conductivity of the sample is given by Equation (55):

$$\sigma_a = \frac{LI}{AV} \tag{55}$$

where I is the applied current, and V is the potential difference measured between the two electrodes.

Another electrode configuration uses two long current electrodes oriented parallel to the cylinder axis on diametrically opposing sides of the cylindrical sample, with two radial point contacts for the measurement of the potential difference located on the surface of the cylindrical sample at the midpoint of both current electrodes and separated radially from them. A cross-sectional view of the sample with the electrodes is shown in Figure 10 [B11.2]. The electrodes are positioned on the inside of a plastic sheath. This method allows resistivity measurements to be made without cutting the core. If the angle between the current electrodes and the potential electrodes is φ, then the apparent conductivity σ_a is given by Equation (56):

$$\sigma_a = \frac{KI}{bV} \tag{56}$$

where b is the length of the current strips, and the geometric factor K is given by Equation (57):

$$K = \frac{1}{\pi}\ln\left[\frac{1+\cos\varphi}{1-\cos\varphi}\right] \tag{57}$$

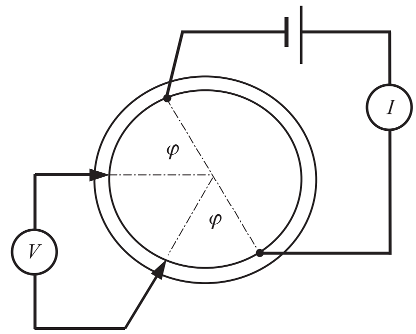

Figure 10—Electrode configuration for resistivity measurements on continuous rock cores

11.2 Practical considerations

The major problem lies in the minimization of the contact resistance for the end-cap electrodes. Tin foil, mercury, and solder have all been used to maximize the contact area. The power source used is either dc or ELF ac [B11.2].

The method has also been used for the semiautomatic measurement of the complex permittivity of ice cores at frequencies up to 50 kHz [B11.1]. Both the conductivity and permittivity are determined in this case.

12. Capacitance methods

12.1 Theory

Capacitance methods represent one of the most fundamental approaches to the measurement of both permittivity and conductivity (see Clause 1). A sample is machined to have two parallel faces, electrodes of a known area are placed on these two faces, and the complex impedance between the plates is measured using an impedance bridge or network analyzer. The complex relative permittivity is determined directly from the measurement of the capacitance [B12.2, B12.3].

12.2 Experimental procedure

A sample of the material is machined to have two parallel, flat surfaces before being inserted between the two parallel plates of a capacitor. The real and imaginary parts of the impedance of the capacitor can be measured using a complex impedance bridge at low frequency and a network analyzer at higher frequencies.

At the Naval Research Laboratories [B12.1], an inductance, capacitance, and resistance (LCR) meter dielectric test fixture was modified to include polished, 10 cm diameter parallel plates with concentric guard rings. One plate is fixed and the other driven by a micrometer drive to ensure accurate thickness determination. The total impedance of the plates, with and without the sample, is measured using an LCR meter. The measured capacitance C_m is given by Equation (58):

$$C_m = C_S + C_{\mathrm{air}} \tag{58}$$

where C_S is the sample capacitance, and C_{air} is the capacitance in air. The real part of the complex permittivity ε' is given by Equation (59):

$$\varepsilon' = \frac{C_m t - \varepsilon_0 A_A}{\varepsilon_0 A_S} \tag{59}$$

where A_S is the area of the electrodes in contact with the sample, and A_A is the area of the air in contact with the electrodes. The sample thickness is t.

The imaginary part of the complex permittivity ε'' is given by Equation (60):

$$\varepsilon'' = \varepsilon' \cdot D_m \tag{60}$$

where D_m is the measured dissipation factor (i.e., the inverse of the quality factor Q).

The sources of error in making these measurements include poor contact between the electrodes and the specimen, and the accurate determination of the sample area A_S. Poor electrical contact can be avoided to some extent by using silver paint on the parallel faces of the sample. For highly conductive materials, the electrode polarization effects can strongly influence ε'' measurements.

A similar technique has been used for many years in investigating polarization processes in rocks [B12.4].

When ice cores are analyzed for variations in conductivity resulting from ancient geological events, a rapid scanning technique is required. The precision of the measurement and the speed of the measurement can be greatly improved using a small movable electrode surrounded by a guard plate, with the other electrode being the container in which the core sample is placed [B12.5]. The second electrode is effectively of infinite length. This technique has been used over the frequency range 30 Hz–1 MHz.

13. Transmission line methods (laboratory)

13.1 Theory

Clause 13 is confined to measurement techniques in the frequency domain. As some transmission line techniques employ TDR techniques, the reader is referred to Clause 9 for a description of these methods.

In investigating the electromagnetic properties of earth materials related to ground probing radar, the open-ended coaxial line technique was regarded as the most useful [B13.9, B13.10]. Above 100 MHz, measurements can be made using small samples with a single flat surface. Below 100 MHz, the capacitive method (Clause 12) was found to be more accurate. The real and imaginary parts of the complex permittivity are given by Equation (61) and Equation (62) [B13.10]:

$$\varepsilon_r' = \frac{-2\Gamma \sin\phi}{\omega C_{\text{air}} Z_0 (1 + 2\Gamma\cos\phi + \Gamma^2)} - \frac{C_f}{C_{\text{air}}} \tag{61}$$

$$\varepsilon_r = \frac{1 - \Gamma^2}{\omega C_{\text{air}} Z_0 (1 + 2\Gamma\cos\phi + \Gamma^2)} \tag{62}$$

where

Γ is the magnitude of the reflection coefficient,

ϕ is the phase of the reflection coefficient,

Z_0 is the characteristic impedance of the line,

C_{air} is the capacitance of the open-ended coaxial line in air,

C_f is the internal fringing capacitance of the coaxial line,

C_{air} is a function of the coaxial cable geometry, which can be determined by calibration against known standards [B13.7].

Full-mode models of the open-ended probe are available [B13.2, B13.6].

The Fourier transform of an electromagnetic pulse fired along a coaxial cable containing a machined annular disk of material has also been used [B13.8]. The pulses have to have a subnanosecond rise time for the frequency coverage required. These measurements yield results that span the frequency range 0.4 – 10 GHz, and provide both complex permittivity and complex permeability of the sample.

Soil measurements can be made by inserting the soil sample into a section of coaxial line with an open-circuited center conductor [B13.1, B13.3].

13.2 Measurement techniques

Open-circuit coaxial probes are available commercially. A typical dielectric probe consists of an open-circuit coaxial cable with an outer circular flange. The flange is pressed against the sample of the material that has been machined flat and the reflection from the open circuit determined using an impedance bridge. As most samples are quite lossy, and as the fringing fields are quite tightly confined to the center conductor and the flange, very small samples can be used [B13.5]. The unit is calibrated over the frequency of measurement using a three-point calibration procedure. Measurements are made in air, against a short circuit, and with a user defined standard (usually water or alcohol) [B13.4]. During a measurement, the complex reflection coefficient is determined across the frequency range, using a vector network analyzer. Also, changes in moisture content and sample compaction can result in laboratory measured values that are different from corresponding in-situ values.

Other major errors in these laboratory measurements include the feed cable mechanical stability, the presence of air gaps between the flange and the sample, and problems created when the sample is too thin [B13.4]. The manufacturer provides an uncertainty factor for the measurement [B13.1]. The largest uncertainty occurs at the lowest frequency due to the size of the probe [B13.7].

The errors in the annular disk method [B13.1] primarily relate to the low voltage (120 mV, 30 ps rise time) and therefore to the low-power density at high frequencies.

14. Waveguide methods

14.1 Theory

A number of approaches to the measurement of the electrical properties of earth materials in the microwave region of the spectrum have employed the use of rectangular metallic waveguides. These laboratory techniques require the insertion of a machined rock sample into the waveguide and the measurement of the reflection coefficient and/or the transmission coefficient. The reflection coefficient measurements use either a traveling waveguide mode or the sample is located in a resonant cavity.

In one method, the specimen is machined to a precise block to fit inside the rectangular waveguide along one plane (either E plane or H plane) with the major part of the waveguide remaining air filled [B14.1]. The wavelength and the attenuation in the waveguide are measured using a slotted line or network analyzer, and the complex relative permittivity of the material is determined. Solving for the complex permittivity requires the iterative solution of a set of transcendental equations [B14.7].

This technique has also been used in the investigation of soils at microwave frequencies [B14.6]. An alternative technique locates the sample in a short-circuited waveguide [B14.3–B14.5] and measurements are made over the frequency range 1–12.2 GHz.

A third method of measurement is to machine the sample to a relatively thin sheet, and the open ends of a waveguide are placed on either side of the material [B14.8]. If the alignment is sufficiently accurate, it is possible to measure both the transmission and reflection (S_{11} and S_{21}) of the signal through the material in the frequency ranges 1.12–1.7 GHz and 8.2–12.4 GHz.

A fourth method employed is to locate the end of the waveguide on the machined side of the rock material. The total reflection coefficient is then measured and inverted to give the effective conductivity and relative permittivity.

In yet another method, the machined sample is positioned in a resonator and measurements are made at a single frequency [B14.2]. It is necessary for the sample to fill a substantial portion of the resonator to ensure adequate coupling to the material. The method is only suited to low-loss materials where the resulting frequency shift of the resonator is less than 1% of its original value.

14.2 Measurement techniques

For low-loss material, an analytical solution is available [B14.1], but this fails when the loss is significant. In Nelson et al. [B14.5], the standing wave ratio (SWR) is measured using an inductive loop or a capacitively coupled probe. The system required calibration in air in front of the sample terminated with a short-circuit. The subsequent analysis takes into account the wall losses as well as losses in the sample itself. At high frequencies, the propagation can support a number of different propagation modes, and this will render the analysis inaccurate.

When using a thin specimen [B14.8], data inversion again requires an interactive technique to deduce values for the complex relative permittivity.

All of these techniques suffer from problems associated with the difficulty in ensuring a good metal–rock contact that is free of air gaps, the difficulties in machining rock without altering the surface of the rock with polishing material, etc. Also, it is important to minimize the development of spurious waveguide modes that are not accounted for in the inversion equations. This last problem is usually solved by ensuring that the transmission path in the material is much less than one wavelength in the material.

15. Free-space reflection and transmission

15.1 Theory

In an attempt to quantify the reflection coefficient of soils and other earth surfaces for aircraft and satellite remote sensing, a number of research groups have undertaken reflection measurements in open fields at frequencies above 10 GHz. The basic premise is that, with a measurement of the complex reflection coefficient as a function of angle of incidence or as a function of the frequency at normal incidence, one can apply Fresnel's laws of reflection to determine the intrinsic impedance of the earth. The technique is used both for an intact surface (i.e., soil where roughness is a factor) or a machined rock sample [B15.1, B15.2, B15.4].

One method is implemented by varying the geometry between the transmitting and receiving antennas so that the received signal level of the space wave (the vector sum of the direct and ground-reflected rays) as a function of elevation angle goes through at least one minimum and one maximum as the angle of incidence is varied. The peak-to-null ratio (PNR) can be related to the modulus of the Fresnel reflection coefficient Γ using a two-ray model for reflection from a planar surface. The phase of the reflection coefficient can be estimated from the elevation angle of the null(s). The complex permittivity (and hence the relative permittivity and conductivity) of the earth's surface in the reflection area (the first Fresnel zones) can be derived from the complex reflection coefficient [see Equation (16) and Equation (17)]. The PNR in decibels is given by Equation (63):

$$PNR = 20\log\left(\frac{1+|\Gamma|}{1-|\Gamma|}\right) \qquad (63)$$

The ground-reflected ray and the direct ray arriving at an antenna located at height h above the ground, differ in phase by φ as a result of the physical path distance, as shown by Equation (64):

$$\varphi = \frac{4\pi h \cos\theta}{\lambda} \qquad (64)$$

There is also a phase shift φ_Γ associated with the Fresnel reflection coefficient.

A null occurs at the angle θ_{null}, when $\varphi_r + \varphi = -180°$. Thus, Equation (63) and Equation (64) are required to solve for σ and ε_r.

It should be emphasized that the reflection coefficient is very much dependent on surface roughness so it is quite difficult to separate out the two effects (i.e., complex permittivity and surface roughness) when the surface is not smooth for the wavelength and angle of incidence of interest.

If a thin sheet of material is used, both the transmission and reflection coefficients can be determined at frequencies up to 110 GHz, using horn antennas with Fresnel lenses [B15.5].

15.2 Experimental methods

Ghodgaonkar et al. [B15.1] made laboratory-based measurements on rock samples using a pair of spot-focusing horn lens antennas with a focal distance-to-diameter ratio of unity. The measurements were conducted in the frequency range 14–17 GHz. Diffraction at the edges of the sample is insignificant because of this focusing. The system is calibrated by measuring the scattering parameters in free space using the transmission reflection line (TRL) technique (through connection, a short-circuit on each port, and a transmission line between the two ports). Assuming plane wave propagation, the reflection from the sample mounted on a metallic backing plate is measured. These data are then used in a computer program, and the problem is solved iteratively.

Three experimental methods have been employed to measure the planar Fresnel reflection coefficient: ground-based measurements, and measurements involving airborne and satellite mounted systems. In the ground-based method, the transmitting and receiving antennas are erected with a horizontal separation distance r sufficient to satisfy the far-field criteria, as shown in Equation (65):

$$r > \frac{2D^2}{\lambda} \qquad (65)$$

where D is twice the height of the antenna above the ground plane, and λ is the free-space wavelength.

The received signal level is recorded as one of the antennas (usually the transmitting antenna) is raised and lowered to vary the angle of incidence θ. The transmitting and receiving antennas have to have a sufficiently broad beamwidth to ensure that the radiated amplitudes of the direct and reflected rays are essentially equal.

In the airborne method, a transmitter on an aircraft is flown over the site while being tracked so that θ is known for the set of received signal levels recorded on the ground.

Kavak et al. [B15.3] monitored the signal strength into a horizontally oriented global positioning system (GPS) receiving antenna as a function of time. The measurements were conducted at 1.6 GHz. As the satellite passes across the sky, the direct ray and the ground-reflected ray interfere. The resultant interference pattern can be analyzed to provide the complex permittivity values of the ground in front of the receiver. A least squares parameter optimization method was used to derive the electrical parameters of the earth's surface. One potential problem with the method is the surface roughness, which, if greater than $\lambda_0/10$, will result in a significant error in the analysis.

It is important to note that major errors can occur as a result of

a) Surface roughness.
b) Lateral variations in the electrical properties of the earth (note that as the angle of incidence changes, so too does the location of the Fresnel zones).
c) Nonuniform antenna polar pattern of both transmitting and receiving antennas.
d) Polarization variations between transmitting and receiving antennas and from the reflecting surface.
e) In the case of long propagation paths, the influence of dynamic changes in the atmospheric propagation path, which could change the angle of incidence.

16. Microwave and millimeter wave remote sensing

16.1 Theory

There are two principal methods of microwave and millimeter wave remote sensing of the earth's surface: passive and active. A passive system detects the radiation from the earth's surface and, from its spectral energy and polarization, it makes determinations about the electromagnetic properties of the ground. It is not possible, however, to determine directly the electrical constants of the ground from these measurements. Passive systems have been employed to deduce the soil moisture profile of soils [B16.8] and sea ice salinity [B16.7], although the permittivity is not measured directly.

One example of a multidimensional approach to the remote sensing of the environment was the aircraft-based microwave assessment of sea ice [B16.2, B16.5]. In this system, images of the surface were obtained using two synthetic aperture radar (SAR) systems operating at 5.3 GHz and 9.25 GHz with two polarizations (horizontal and vertical), and these data were correlated with an airborne imaging radiometer operating at 37 GHz and 90 GHz (two polarizations). From these data, the complex relative permittivity properties of the newly formed sea ice were determined.

An active system requires illumination of the earth's surface with electromagnetic radiation and the detection of the reflected energy. The intensity of the reflected components is dependent on the polarization, frequency, depression angle, the complex permittivity of the earth [Equation (16) and Equation (17)], and the surface roughness. The earth's electrical parameters can be determined from these measurements, although these are rarely extracted in routine remote sensing applications.

An example of an active remote sensing system involves the use of an airborne or spacecraft-based radar system (e.g., SAR). The complex permittivity of soil has been determined to a depth of 40 cm [B16.1] and of surface water salinity [B16.4] at 30 MHz using radar.

16.2 Field methodology

Radar pulses are directed towards the earth from the aircraft or spacecraft in a fan-shaped beam oriented normal to the direction of flight. The reflected pulse from directly beneath the aircraft arrives first followed by those at an angular displacement. Using the coherent addition of the signals, it is possible to synthesize a very large effective aperture. The operation of this radar at microwave frequencies allows cloud penetration. Different types of rock can be distinguished by their depolarization characteristics. The radar signal can penetrate a short distance into vegetation cover and also into low-conductivity soils and ice.

For soil moisture profiling, the platform was an aircraft flown at an elevation of 500 to 1000 m with a flight speed of 180 to 190 km/h. The carrier frequency of the transmitter was 30 MHz with a pulse length of 1 μs with a repetition frequency of 1 kHz. Side reflections were removed using time gating. The parameters recorded were the mean electric field amplitude (measured with crossed dipole antennas), the modulation coefficient, and the characteristic fluctuation time. The last two parameters allow for the removal of surface roughness effects. The system was calibrated over a quiet water body of known complex permittivity. The soil permittivity was then estimated from the Fresnel reflection coefficients [Equation (16) and Equation (17)].

There is a significant problem in determining and removing the effect of surface roughness [B16.3, B16.6, B16.9].

Annex A

(informative)

List of symbols

α attenuation constant (real part of the complex propagation constant)

β phase constant (imaginary part of the complex propagation constant)

γ complex propagation constant ($\gamma = \alpha + j\beta$)

$\Gamma_{||}$ TM Fresnel reflection coefficient

$\Gamma_{\perp}$ TE Fresnel reflection coefficient

Γ reflection coefficient of transmission line in time domain reflectometry

Γ magnitude of the reflection coefficient in transmission line methods

δ skin depth (m)

$\delta(\theta)$ normalized surface admittance

Δ normalized impedance

ε permittivity (F/m)

ε_0 permittivity of free space ($\varepsilon_0 = 8.854 \times 10^{-12}$ F/m)

ε_r complex relative permittivity

ε_r' real part of the complex relative permittivity

ε_r'' imaginary part of the complex relative permittivity

θ_i angle of incidence measured with respect to the surface normal

θ_t angle of transmission measured with respect to the surface normal

λ free-space wavelength (m)

μ magnetic permeability (H/m)

μ_0 magnetic permeability of free space ($\mu_0 = 4\pi \times 10^{-7}$ H/m)

ρ resistivity (Ωm)

ρ_a apparent resistivity (Ωm)

σ conductivity (S/m)

φ	angular location of current electrode in laboratory resistivity method
φ	phase pathlength in waveguide methods
φ_r	phase shift resulting from Fresnel reflection
ϕ	phase of reflection coefficient
ω	angular frequency (rad/s)
a	electrode spacing factor (m)
a_2	constant
A_A	area of the air in contact with electrodes
A_S	area of electrodes in contact with sample
b	length of current electrodes in laboratory resistivity method
b_1	constant
b_2	constant
B	susceptance (S) (imaginary part of the admittance)
c	velocity of light in free space
C	capacitance (F)
C_0	capacitance per unit length in probe impedance method
C_{0b}	capacitance of probe in borehole material
C_{0g}	capacitance of probe in ground near borehole
C_{air}	capacitance of probe measured in air
C_f	fringing capacitance
C_m	measured capacitance
C_{ground}	capacitance of probe measured in the ground
d	separation distance between transmitting and receiving antenna
D	twice the height of the antenna above the ground plane
D	dissipation factor in a capacitance measurement
D_m	measured dissipation factor
E_V	vertical electric field component

E_x electric field component in the X direction

E_y electric field component in the Y direction

f frequency (Hz)

G conductance (real part of admittance) (S)

h reference depth (m) (for TEM applications)

h_1 depth/thickness/height of layer 1 or probe

H_x magnetic field component in the X direction

H_y magnetic field component in the Y direction

I current (A)

I_0 modified Bessel function of order 0

I_1 modified Bessel function of order 1

j imaginary number ($j = \sqrt{-1}$)

k wavenumber

k_0 wavenumber in free space

K geometric factor for resistivity measurements

K_0 modified Bessel function of order 0

K_1 modified Bessel function of order 1

l length (m)

L length of transmission line (m)

m integer value

n integer value

p numerical distance (factor in Sommerfeld attenuation function W)

PNR peak-to-null ratio

q_1 factor in Sommerfeld attenuation function W

q_2 factor in Sommerfeld attenuation function W

Q charge (C)

Q_1 multiple layer factor

r separation distance (m)

r radius (m)

R resistance (real part of impedance) (Ω)

R_E electrode resistance (Ω)

t time (s) (for TEM applications)

t sample thickness

TE transverse electric

TM transverse magnetic

u_1 complex propagation constant in the direction of the surface normal

V voltage (V)

W Sommerfeld attenuation function

W_e electric wave tilt

W_m magnetic wave tilt

X reactance (imaginary part of impedance) (Ω)

Y admittance (S) ($Y = G + jB$)

Y_1 surface admittance of Medium 1 assuming infinite depth

Y_b admittance contribution from borehole

Y_g admittance contribution from ground

Y_S surface admittance

Z impedance (Ω) ($Z = R + jX$)

Z intrinsic impedance of medium

Z impedance of transmission line in time domain reflectometry

Z surface impedance tensor (2×2) array of complex numbers

Z_0 intrinsic impedance of free space ($Z_0 = 120\pi\Omega$)

Z_1 intrinsic impedance of Medium 1

Z_n intrinsic impedance of Medium n

Z_S surface impedance

$\hat{Z}$ effective impedance

Annex B

(informative)

Bibliography

Clause 1

[B1.1] Ahrens, T.J. (ed.), *Mineral Physics and Crystallography, A Handbook of Physical Constants*. Washington, DC: American Geophysical Union, 1995.

[B1.2] Brown, J. "Artificial dielectrics," *Progress in Dielectrics*, vol. 2, pp. 195–225, 1960.

[B1.3] Cheng, D.K. *Field and Wave Electromagnetics*, 2nd ed., Reading, MA: Addison Wesley, 1989, p. 216.

[B1.4] Cole, K.S. and Cole, R.H. "Dispersion and absorption in dielectrics," *Journal of Chemical Physics*, vol. 9, pp. 341–351, 1941.

[B1.5] deBettencourt, J.T., Davidson, D., and Wait, J.R. "IEEE guide for radio methods of measuring earth conductivity," *IEEE Transactions on Antennas and Propagation*, vol. 22, no. 2, pp. 373–400, Mar. 1974.

[B1.6] IEEE Std 211-1997™, Definition of Terms for Radio Wave Propagation.

[B1.7] IEEE Std 356-1974™, IEEE Guide for Radio Methods of Measuring Earth Conductivity.

[B1.8] ITU-R Recommendation P. 527-3, "Electrical characteristics of the surface of the Earth," *ITU-R Recommendations, P Series, Radiowave Propagation*, 2000.

[B1.9] ITU-R Recommendation P. 832-2, "World atlas of ground conductivities," *ITU-R Recommendations*, *P Series, Radiowave Propagation*, 2000.

[B1.10] Keller, G.V. and Frischknecht, F.C. *Electrical Methods in Geophysical Prospecting*, Oxford, U.K.: Pergamon Press, 1966.

[B1.11] King, R.W.P. and Smith, G.S. *Antennas in Matter*, Cambridge, MA: MIT Press, 1981.

[B1.12] Levitskaya, T.M. and Sternberg, B.K. "Polarization processes in rocks. 2. Complex electrical resistivity method," *Radio Science*, vol. 31, pp. 781–802, Jul.–Aug. 1996.

[B1.13] Longmire, G.L. and Smith, K.S. "A universal impedance for soils," Topical Report for period 1 July 1975 to 30 Sept. 1975, Report No. MRG-N-214, Contract DNA 001-75-6-0094, Mission Research Corporation, Santa Barbara, CA, Oct. 1975.

[B1.14] Lytle, R.J. "Measurement of earth medium electrical characteristics: techniques, results and applications," *IEEE Transactions on Geoscience and Electronics*, vol. 12, no. 3, pp. 81–101, 1974.

[B1.15] Nabighian, M.N. (ed.), *Electromagnetic Methods in Applied Geophysics*. vol. 1, *Theory*, Tulsa, OK: Society of Exploration Geophysicists, 1988.

[B1.16] Negi, J.G. and Saraf, P.D. "Impedance of a plane electromagnetic wave at the surface of a layered conducting earth with dipping anisotropy," *Geophysical Prospecting*, vol. 20, pp. 785–799, 1972.

[B1.17] Okoniewski, M., Mrozowski, M., and Stuchly, M.A. "Simple treatment of multi-term dispersion in FDTD," *IEEE Microwave & Guided Wave Letters*, vol. 7, pp. 121–123, May 1997.

[B1.18] Oldenburg, D.W. "Practical strategies for the solution of large-scale electromagnetic inverse problems," *Radio Science*, vol. 29, no. 4, pp. 1081–1099, Jul.–Aug. 1994.

[B1.19] Sternberg, B.K. and Levitskaya, T.M. "Correlation between laboratory and in-situ electrical resistivity measurements of soil," *Journal of Environmental and Engineering Geophysics*, vol. 3, no. 2, pp. 63–70, Jun. 1998.

[B1.20] Sullivan, D.M. "Z-transform theory and the FDTD method," *IEEE Transactions on Antennas and Propagation*, vol. 44, pp. 28–34, Jan. 1996.

[B1.21] Taylor, L.S. "Dielectric properties of mixtures," *IEEE Transactions on Antennas and Propagation*, vol. 13, no. 16, pp. 943–947, Nov. 1965.

[B1.22] Thiel, D.V. Comments on "Effect of inclined anisotropic substratum on magnetotelluric response" by Singh, R.P. *Geophysical Prospecting*, vol. 34, pp. 923–924, 1986.

[B1.23] Wait, J.R. "Effective electrical properties of heterogeneous earth models," *Radio Science*, vol. 18, pp. 19–24, 1983.

[B1.24] Wait, J.R. "Complex resistivity of the earth," *Progress in Electromagnetic Research*, vol. 1, pp. 1–175, 1989.

[B1.25] Wait, J.R. *Electromagnetic Waves in Stratified Media*, Piscataway, NJ: IEEE Press, 1996.

[B1.26] Wait, J.R. "Electromagnetic response of an anisotropic half-space model when the medium striations are tilted relative to the vertical," *Journal of Electromagnetic Waves and Applications*, vol. 10, no. 6, pp. 871–881, 1996.

[B1.27] Wang, J.R. "The dielectric properties of soil–water mixtures at microwave frequencies," *Radio Science*, vol. 15, pp. 977–985, Sept.–Oct. 1980.

Clause 2

[B2.1] Bentley, C.R. "Electrical resistivity measurements on the Ross Ice Shelf," *Journal of Glaciology*, vol. 18, no. 78, pp. 15–35, 1977.

[B2.2] Daily, W. and Owen, E. "Cross borehole resistivity tomography," *Geophysics*, vol. 56, pp. 1228–1235, Aug. 1991.

[B2.3] deBettencourt, J.T., Davidson, D., and Wait, J.R. "IEEE guide for radio methods of measuring earth conductivity," *IEEE Transactions on Antennas and Propogation*, vol. 22, no. 2, pp. 373–400, Mar. 1974.

[B2.4] Hubbard, B., Binley, A., Slater, L., Middleton, R., and Kulessa, B. "Inter-borehole electrical resistivity imaging of englacial drainage," *Journal of Glaciology*, vol. 44, no. 147, pp. 429–434, 1998.

[B2.5] Keller, G.V. and Frischknecht, F.C. *Electrical Methods in Geophysical Prospecting*, Oxford: Pergamon Press, 1966.

[B2.6] Lu, K. and Macnae, J. "The international campaign on intercomparison between electrodes for geoelectrical measurements," *Exploration Geophysics*, vol. 29, pp. 484–488, 1998.

[B2.7] Merrick, N.P. "A schema for the direct interpretation of electrical resistivity soundings," *Exploration Geophysics*, vol. 20, pp. 469–479, 1989.

[B2.8] Merrick, N.P. and Poezd, E. "RINVERT for Windows; software for the interpretation of resistivity soundings," *Exploration Geophysics*, vol. 28, pp. 110–113, 1997.

[B2.9] Mufti, I.R. "Finite difference resistivity modeling for arbitrary shaped two dimensional structures," *Geophysics*, vol. 41, pp. 62–78, Feb. 1976.

[B2.10] Parasnis, D.S. *Mining Geophysics*, 2nd ed. Amsterdam: Elsevier, 1976.

[B2.11] Sasaki, Y. "3D resistivity inversion using the finite-element method," *Geophysics*, vol. 59, pp. 1839–1848, Dec. 1994.

[B2.12] Scott, W.J. and Maxwell, F.K. "Marine resistivity survey for granular materials, Beaufort Sea," *Canadian Journal of Exploration Geophysics*, vol. 25, pp. 104–114, Dec. 1989.

[B2.13] Shima, H. "Two dimensional automatic resistivity inversion technique using alpha centers," *Geophysics*, vol. 55, pp. 682–694, Jun. 1990.

[B2.14] Telford, W.M., Geldart, L.P., Sheriff, R.E., and Keys, D.A. *Applied Geophysics*, London: Cambridge University Press, 1976.

[B2.15] Van Blaricom, R. *Practical Geophysics II for the Exploration Geologist*, Spokane, WA: Northwest Mining Association, 1992.

[B2.16] Wait, J.R. *Geoelectromagnetism*. New York: Academic Press, p. 63, 1982.

[B2.17] Wait, J.R. "Complex resistivity of the earth," *Progress in Electromagnetics Research,* vol. 1, pp. 1–175, 1989.

[B2.18] Wait, J.R. and Conda, A.M. "On the measurement of ground conductivity at VLF," *IRE Transactions on Antennas and Propagation*, vol. 6, pp. 273–277, Jul. 1958.

[B2.19] Zhang, J., Mackie, R.L., and Madden, T.R. "3D resistivity forward modeling and inversion using conjugate gradients," *Geophysics*, vol. 60, pp. 1313–1325, Sept.–Oct. 1995.

Clause 3

[B3.1] Benderitter, Y., Joliuet, A., Mounin, M., and Tabbagh, A. "Application of the electrostatic quadrapole to sounding in the hectometric range," *Journal of Applied Geophysics*, vol. 31, pp. 1–6, 1994. Comments by J.R. Wait, vol. 34, pp. 78–80, 1995.

[B3.2] Cagniard, L. "Basic theory of the magnetotelluric method of geophysical prospecting," *Geophysics*, vol. 18, no. 3, pp. 605–635, July 1953. Comments by J.R. Wait, vol. 19, pp. 281–289, 1954.

[B3.3] Collett, L.S. and Jensen, O.G. (eds.), Geophysical applications of surface wave impedance measurements," *Geological Survey of Canada*, Paper no. 81 15, 1982.

[B3.4] Goldstein, M.A. and Strangway, D.W. "Audio-frequency magnetotellurics with a grounded electric dipole source," *Geophysics*, vol. 40, pp. 669–683, 1975.

[B3.5] Hohmann, G.W. "Three dimensional EM modeling," *Geophysical Surveys*, vol. 6, pp. 27–53, 1983.

[B3.6] Kato, Y. and Kikuchi, T. "On the phase difference of earth current induced by the changes of the earth's magnetic field," *Science Reports of Tohoku University*, *Series V*, *Geophysics*, vol. 2, pp. 139–145, 1950.

[B3.7] Ku, C.C. "Numerical inverse magnetotelluric problems," *Geophysics*, vol. 41, pp. 276–286, Apr. 1976.

[B3.8] Mackie, R.L., Maddern, T.R., and Wannamaker, P.E. "Three-dimensional magnetotelluric modeling using difference equations – Theory and comparison to integral equation solutions," *Geophysics*, vol. 58, no. 2, pp. 215–226, 1993.

[B3.9] Porstendorfer, G. *Principles of Magnetotelluric Prospecting*, Berlin-West, Stuttgart: Gebrüder Bornträger, 1975.

[B3.10] Reddy, I.K., Rankin, D., and Phillips, R.J. "Three-dimensional modeling in magnetotelluric and magnetic variational sounding," *Geophysics Journal of Royal Astronomical Society*, vol. 51, pp. 313–315, 1977.

[B3.11] Silvester, P. and Haslam, C.R.S. "Magnetotelluric modeling by the finite element method," *Geophysics Prospecting*, vol. 4, no. 2, pp. 872–891, 1972.

[B3.12] Strangway, D.W., Swift, C.M. Jr., and Holmer, R.C. "The application of audio-frequency magnetotellurics (AMT) to mineral exploration," *Geophysics*, vol. 38, no. 6, pp. 1159–1175, 1973.

[B3.13] Thiel, D.V. and Mittra, R. "Surface impedance modeling using the finite-difference time-domain method," *IEEE Transactions on Geoscience and Remote Sensing*, vol. 35, no. 5, pp. 1350–1356, Sept. 1997.

[B3.14] Thiel, D.V. and Mittra, R. "An analysis of a staked dipole probe on a lossy earth plane using the finite difference time domain method," *IEEE Transactions on Geoscience and Remote Sensing*, vol. 35, no. 5, pp. 1357–1362, Sept. 1997. Comments by J.R. Wait, Jan. 1999.

[B3.15] Thiel, D.V., Wilson, M.J., and Webb, C.J. "A surface impedance mapping technique based on radiation from discrete lightning strokes," *Geoexploration*, vol. 25, pp. 163–172, 1988.

[B3.16] Tikhonov, A.N. "Determination of the electrical characteristics of deep strata of the earth's crust," *Doklady Akademii Nauk SSSR* (in Russian), vol. 73, no. 2, pp. 295–297, 1950.

[B3.17] Ting, S.C. and Hohmann, G.W. "Integral equation modeling of three-dimensional magnetotelluric response," *Geophysics*, vol. 46, pp. 182–197, 1981.

[B3.18] Wait, J.R. *Electromagnetic Waves in Stratified Media*, 2nd ed. New York: Pergamon Press, 1970.

[B3.19] Weidelt, P. "Electromagnetic induction in three dimensional structures," *Journal of Geophysics*, vol. 41, pp. 85–109, 1975.

[B3.20] Whittall, K.P. and Oldenburg, D.W. "Inversion of magnetotelluric data for a one dimensional conductivity," Geophysical Monograph Series no. 5., Tulsa, OK: Society of Exploration Geophysicists, 1992.

[B3.21] Zonge, K.L. and Hughes, L.J. "The effect of electrode contact resistance on electric field measurements," *SEG 55th Annual Convention*, Washington, DC, Oct. 1985.

For Further Reading

[B3.22] Nabighian, M.N. (ed.), *Electromagnetic Methods in Applied Geophysics*, vol. 2, *Application, Part B*, Tulsa, OK: Society of Exploration Geophysicists, 1991.

[B3.23] Patra, H.P. and Mallick, K. *Geosounding Principles: Time Varying Geoelectric Soundings (Methods in Geochemistry and Geophysics Series)*, vol. 14B, New York: Elsevier, 1980.

[B3.24] Thiel, D.V. "A preliminary assessment of glacial ice profiling using surface impedance measurements," *Journal of Glaciology*, vol. 32, no. 112, pp. 376–382, 1986.

[B3.25] Thiel, D.V. and Neall, F.B. "VLF surface impedance measurements in the Antarctic," *Journal of Glaciology*, vol. 35, no. 120, pp. 197–200, 1989.

[B3.26] Vozoff, K. (ed.), *Magnetotelluric Methods*, Tulsa, OK: Society of Exploration Geophysicists, 1985.

[B3.27] Wait, J.R. *Geoelectromagnetism*, New York: Academic Press, 1982.

Clause 4

[B4.1] Berry, L.E. "Radio propagation over a Gaussian-shaped ridge," *IEEE Transactions on Antennas and Propagation*, vol. 15, pp. 701–702, Sept. 1967.

[B4.2] deBettencourt, J.T. and Frazier, J.W. "Rock electrical characteristics deduced from depth attenuation rates (in drill holes)," *IEEE Transactions on Antennas and Propagation*, vol. 11, pp. 358–363, May 1963.

[B4.3] Durkin, J. "Earth conductivity estimates from through-the-earth electromagnetic transmission tests," *IEEE Transactions on Geoscience and Remote Sensing*, vol. 29, no. 2, pp. 300–307, 1991.

[B4.4] IEEE Std 291-1991™, Standard Methods for Measuring Electromagnetic Field Strength of Sinusoidal Continuous Waves, 30 Hz to 30 GHz.

[B4.5] Keller, G.V. and Frischknecht, F.C. *Electrical Methods in Geophysical Prospecting*, Oxford: Pergamon Press, 1966, Chapter 7.

[B4.6] Kong, J.A., Tsang, L., and Simmons, G. "Geophysical subsurface probing with radio-frequency interferometry," *IEEE Transactions on Antennas and Propagation*, vol. 22, pp. 616–620, Jul. 1974.

[B4.7] Koskenniemi, O. and Laiho, J. "Measurement of the effective ground conductivity at low and medium frequencies in Finland," *EBU Reviews in Technology*, vol. 153, pp. 237–240, Oct. 1975.

[B4.8] Longley, A.G. "Radio propagation in urban areas," *Proceedings of 28th IEEE Vehicular Technology Conference*, Mar. 1978, pp. 503–511.

[B4.9] Lui, G., Smith, G., Thomson, S., Vozoff, K., and Hatherly, P. "A numerical study of electromagnetic wave propagation (RIM) in disrupted coal seams," *Exploration Geophysics*, vol. 22, pp. 247–250, 1991.

[B4.10] Lytle, R.J., Laine, E.F., Lager, D.L., and Davis, D.T. "Cross borehole electromagnetic probing to locate high contrast anomalies," *Geophysics*, vol. 44, pp. 1667–1676, Oct. 1979.

[B4.11] Peden, I.C., Webber, G.E., and Chandler, A.S. "Complex permittivity of the Antarctic ice sheet in the VLF band," *Radio Science*, vol. 7, pp. 645–650, Jun. 1972.

[B4.12] Rogers, G., Edwards, S., and Young, J. "Geotomography for the delineation of coal seam structure," *Geoexploration*, vol. 24, pp. 301–328, 1987.

[B4.13] Thomson, S., Neil, M., and Jeffrey, S. "In-mine applications of radio imaging," *Preview*, vol. 59, pp. 21–25, Dec. 1985.

[B4.14] Wait, J.R. "Lateral waves and the pioneering research by the late Kenneth A. Norton, 1907–1992," *The Radio Science Bulletin*, no. 276, p. 35, Mar. 1976.

[B4.15] Wait, J.R., Ott, R., and Telfer, T. *Proceedings of Workshop on Radio Systems in Forested and/or Vegetated Environments*, Technical Report ACC-AC-1-74, Ft. Huachuca, AZ: U.S. Army Communications Command, Feb. 1974.

[B4.16] Wu, Z., Maclean, T.S., Bagwell, D.J., and Mehler, M.J. "Propagation over an inhomogeneous irregular surface," *Radio Science*, vol. 23, pp. 33–40, Jan.–Feb. 1988.

Clause 5

[B5.1] Jordan, E.C. *Electromagnetic Wave and Radiating Systems*, 2nd ed. Englewood Cliffs, NJ: Prentice Hall, 1968, Chapter 16.

[B5.2] King, R.J. "Crossed dipole method of measuring wave tilt", *Radio Science*, vol. 3, no. 4, pp. 345–350, 1968.

[B5.3] King, R.J. "Wave-tilt measurements," *IEEE Transactions on Antennas and Propagation*, vol. 24, no. 1, pp. 115–119, Jan. 1976.

[B5.4] King, R.J. "On airborne wave tilt measurements," *Radio Science*, vol. 12, no. 3, pp. 405–414, May–June 1977.

[B5.5] Kovatrina, T. "Electrical ground constants in Central, Eastern, and North Eastern Thailand," Special Technical Report 29, Contract DA 36-039AMC-00040(E), Menlo Park, CA: Stanford Research Institute, Feb. 1997.

[B5.6] Wait, J.R. *Electromagnetic Waves in Stratified Media*, Piscataway, NJ: IEEE Press, 1996.

Clause 6

[B6.1] Bhattacharyya, B.K. "Input resistances of horizontal electric and vertical magnetic dipoles over a homogeneous ground," *IEEE Transactions on Antennas and Propogation*, vol. 11, pp. 261–266, 1963.

[B6.2] Goldstein, N.E., Parker, H.R., and Hagn, G.H. "Three techniques for measurement of ground constants in the presence of vegetation," Stanford Research Institute, Special Technical Report 30, Mar. 1967.

[B6.3] Hagn, G.H. "Ground constants at high frequencies (HF)," *Proceedings of Third Annual Review of Progress in Applied Computational Electromagnetics*, Monterrey, CA: Mar. 1987.

[B6.4] Hagn, G.H. "HF ground constant measurements at the Lawrence Livermore National Laboratory field site," *Applied Computational Electromagnetics Society Journal*, vol. 3, pp. 131–165, 1988.

[B6.5] Hagn, G.H. "Correction factors for SRI International open-wire (OWL) ground constants kit data," *Applied Computational Electromagnetics Society Newsletter*, vol. 6, pp. 35–37, Mar. 1991.

[B6.6] Hagn, G. and Faulconer, J.H. "HF ground constants at the Voice of America (VOA) station at Monrovia, Liberia," *SRI International Report*, June 1985.

[B6.7] King, R.W.P. and Smith, G.S. *Antennas in Matter: Fundamental Theory, and Applications*, Cambridge, MA: MIT Press, 1981.

[B6.8] Kirkscether, E.J. "Ground constant measurements using a section of balanced two-wire transmission line," *IEEE Transactions on Antennas and Propagation*, vol. 8, pp. 307–312, May 1960.

[B6.9] Kobayashi, Y., Okamoto, K., and Yoda, M. "Exploration of archaeological structures in deeper subsurface by means of directive antenna," *Journal of Applied Geophysics*, vol. 35, nos. 2 and 3, pp. 175–183, Oct. 1996.

[B6.10] Nicol, J.L. and Ridd, P.V. "Antenna input impedance: experimental confirmation and geological application," *Canadian Journal of Physics*, vol. 66, pp. 818–823, Sept. 1988.

[B6.11] Peden, I.C. and Rogers, J.C. "An experiment for determining the VLF permittivity of deep Antarctic ice," *IEEE Transactions on Geoscience and Remote Sensing*, vol. 9, pp. 224–233, Oct. 1971.

[B6.12] Rogers, J.C. and Peden, I.C. "The electrically short sheathed dipole: experimental relationship between its measured admittance and the permittivity of the external medium," *IEEE Transactions on Antennas and Propagation*, vol. 21, pp. 857–861, Nov. 1973.

[B6.13] Rogers, J.C. and Peden, I.C. "The VLF complex permittivity of deep Antarctic ice measured in-situ," *Radio Science*, vol. 10, pp. 763–771, Aug.–Sept. 1975.

[B6.14] Scott, W.R. Jr. and Smith, G.S. "Error analysis for dielectric spectroscopy using shielded open-circuited coaxial lines of general length," *IEEE Transactions on Instruments and Measurements*, vol. 35, pp. 130–137, June 1986.

[B6.15] Scott, W.R. Jr. and Smith, G.S. "Dielectric spectroscopy using monopole antennas of general electrical length," *IEEE Transactions on Antennas and Propagation*, vol. 34, pp. 919–929, July 1986.

[B6.16] Smith, G.S. and Nordgard, J.D. "Measurement of the electrical constitutive parameters of materials using antennas," *IEEE Transactions on Antennas and Propagation*, vol. 33, pp. 783–792, July 1985.

[B6.17] Smith, G.S. and Scott, W.R. Jr. "Measurement of the electrical constitutive parameters of materials using antennas, Part II," *IEEE Transactions on Antennas and Propagation*, vol. 35, pp. 962–967, Aug. 1987.

[B6.18] Thiel, D.V. and Stewart, A.J. "The input impedance of electrically short horizontal wire antennas close to the air/earth interface," *Journal of Electrical and Electronic Engineering (Australia)*, vol. 7, no. 4, pp. 252–256, 1987.

[B6.19] Tsao, C.K.H. and DeBettencourt, J.T. "Conductivity measurements in dissipative media with electrically short probes," *IEEE Transactions on Instruments and Measurements*, vol. 16, pp. 242–246, Sept. 1967.

For Further Reading

[B6.20] Banos, A. *Dipole Radiation in the Presence of a Conducting Half Space*, Oxford: Pergamon Press, 1966.

[B6.21] Wait, J.R. *Geoelectromagnetism*, New York: Academic Press, 1982.

[B6.22] Ward, S.H. and Hohman, G.W. "Electromagnetic theory for geophysical applications," in M.N. Nabighian (ed.), *Electromagnetic Methods in Applied Geophysics*, vol. 1, Tulsa, OK: Society of Exploration Geophysicists, 1988, Chapter 4.

Clause 7

[B7.1] Bak, N.H., Sternberg, B.K., Dvorak, S.L., and Thomas, S.J. "Rapid, high-accuracy electromagnetic soundings using a novel four-axis coil to measure magnetic field ellipticity," *Journal of Applied Geophysics*, vol. 30, pp. 235–245, 1993.

[B7.2] Chilingar, G.V., Margot, F.L., Adamson, L.G., Armstrong, R.A., Fertl, W.R., Ershaghi, I., and Hashem, M.N. "Well Logging," in Finkl, C.W. Jr. (ed.), *The Encyclopedia of Field and General Geology*, New York: Van Nostrand Reinhold, 1988, pp. 865–867.

[B7.3] Fraser, D.C. "The multicoil II airborne electromagnetic system," *Geophysics*, vol. 44, pp. 1367–1394, 1979.

[B7.4] Glennie, E.B. and Miller, T.J.E. "Inductive detection of underground metallic pipes," *Proceedings of the Institute of Electrical Engineers (U.K.)*, vol. 122, pp. 345–348, Apr. 1975.

[B7.5] Howard, A.Q. Jr. "Induction logging for vertical structures in the presence of borehole fluids," *Geophysics*, vol. 46, pp. 68–75, Jun. 1981.

[B7.6] Keller, G.V. and Frischknecht, F.C. *Electrical Methods in Geophysical Prospecting*, Oxford: Pergamon Press, 1966, Chapter 6.

[B7.7] Klein, J. and Lajoie, J.J. "Electromagnetics," in R. van Blaricom, *Practical Geophysics II*, Spokane, WA: North West Mining Association, 1992, Chapter 6.

[B7.8] Kovacs, A. and Holladay, J.S. "Sea-ice thickness measurement using a small airborne electromagnetic sounding system," *Geophysics*, vol. 55, pp. 1327–1337, Oct. 1990.

[B7.9] Kovacs, A. and Morey, R.M. "Sounding sea ice thickness using a portable electromagnetic induction instrument," *Geophysics*, vol. 56, pp. 1992–1998, Dec. 1991.

[B7.10] McNeill, J.D. "Electromagnetic terrain conductivity measurement at low induction numbers," Technical Note TN-6, Geonics Ltd., Mississauga, Ont., Canada, Oct. 1980.

[B7.11] McNeill, D. "EM34-3 survey interpretation techniques," Technical Note TN-8, Geonics Ltd., Mississuaga, Ontario, Canada, Nov. 1980.

[B7.12] Spies, B.R. and Frischknecht, F.C. "Electromagnetic Sounding," in Nabighian, M.N. (ed.), *Electromagnetic Methods in Applied Geophysics*, vol. 2, *Applications, Part A*, Tulsa, OK: S.E.G., 1991, Chapter 5.

[B7.13] Sternberg, B.K. and Poulton, M.M. "The LASI high-frequency ellipticity system," *Proceedings of the Environmental and Technical Development through Industry Partnership Meeting*, Department of Energy, Morgantown Energy Technology Center, WV, Oct. 3–5, 1995.

[B7.14] Wait, J.R. *Geoelectromagnetism*, New York: Academic Press, 1982.

[B7.15] Ward, S.H. and Hohmann, G.W. "Electromagnetic theory for geophysical applications," in Nabighian, M.N. (ed.), *Electromagnetic Methods in Applied Geophysics*, vol. 1, *Theory*, Tulsa, OK: S.E.G., 1988.

[B7.16] Worthington, M.H., Kuckes, A., and Oristaglio, M. "A borehole induction procedure for investigating electrical conductivity structure within the broad vicinity of a hole," *Geophysics*, vol. 46, pp. 65–67, Jan. 1981.

Clause 8

[B8.1] Barringer, A.R. "The use of audio and radio frequency pulses for terrain sensing," *Proceedings of Symposium on Remote Sensing of the Environment*, Ann Arbor, MI, 1963, pp. 201–214.

[B8.2] Coggon, J.H. and Clarke, E.H. "The fixed receiver electromagnetic (FREM) method for drill hole surveys," *Exploration Geophysics*, vol. 18, pp. 305–311, 1987.

[B8.3] Macnae, J.C. and Lamontagne, Y. "Imaging quasi-layered conductive structures by simple processing of TEM data," *Geophysics*, vol. 52, pp. 545–554, 1987.

[B8.4] Macnae, J. and McGowan, P. "Quantitative resistance and capacitive electrodes: new developments in inductive source resistivity," *Exploration Geophysics*, vol. 22, pp. 251–256, 1991.

[B8.5] Nabighian, M.N. and McNae, J.C. "TEM systems," in Nabighian, M.N. (ed.), *Electromagnetic Methods in Applied Geophysics*. vol. 2, *Applications*, *Part A*, Tulsa, OK: Society of Exploration Geophysicists, pp. 479–483, 1991.

[B8.6] Raiche, A.P. and Spies, B.R. "Coincident loop transient electromagnetic master curves for interpretation of two layer earths," *Geophysics*, vol. 46, pp. 53–64, Jan. 1981.

[B8.7] Spies, B.R. and Frischknecht, F.C. "Electromagnetic sounding," in Nabighian, M.N. (ed.), *Electromagnetic Methods in Applied Geophysics*. vol. 2, *Applications*, *Part A*, Tulsa, OK: Society of Exploration Geophysicists, pp. 285–425, 1991.

[B8.8] van Blaricom, R. *Practical Geophysics II*, Spokane, WA: North West Mining Association, 1992.

[B8.9] Wait, J.R. *Geoelectromagnetism*, New York: Academic Press, 1982, pp. 177–181.

[B8.10] Wang, T., Oristaglio, M., Tripp, A., and Hohmann, G. "Inversion of diffusion electromagnetic data by a conjugate-gradient method," *Radio Science*, vol. 29, no. 4, pp. 1143–1156, Jul.–Aug. 1994.

[B8.11] Ward, S.H. and Hohmann, G.W. "Electromagnetic theory for geophysical applications," in Nabighian, M.N. (ed.), *Electromagnetic Methods in Applied Geophysics*, vol. 1, *Theory*, Tulsa, OK: Society of Exploration Geophysicists, 1988.

For Further Reading

[B8.12] Keller, G.V. and Frischnecht, F.C. *Electrical Methods in Geophysical Prospecting*, Oxford, U.K.: Pergamon Press, 1966.

[B8.13] Patra, H.P. and Mallick, K. *Geosounding Principles, 2*. Amsterdam: Elsevier, 1980.

Clause 9

[B9.1] Dai, R. and Young, C.T. "Theory and sensing applications of a long antenna on layered media," *Radio Science*, vol. 32, pp. 43–57, Jan.–Feb. 1997.

[B9.2] Garner, S.J., Thiel, D.V., and O'Keefe, S.G. "Surface impedance time domain reflectometry for the determination of ice depth," *Geophysical Research Letters*, vol. 24, pp. 1599–1602, 1997.

[B9.3] Hoekstra, P. and Delaney, A. "Dielectric properties of soils at UHF and microwave frequencies," *Journal of Geophysical Research*, vol. 79, pp. 1699–1708, 1974.

[B9.4] King, R.W.P. and Smith, G.S. *Antennas in Matter*, Cambridge, MA: MIT Press, 1981.

[B9.5] Morey, R.M., Kovacs, A., and Cox, G.F.N. "Electromagnetic properties of sea ice," CRREL Report 84-2, US Army Corps of Engineers, Jan. 1984.

[B9.6] Topp, G.C., Davis, J.L., and Annan, A.P. "Electromagnetic determination of soil water content; measurements in coaxial transmission lines," *Water Resources Research*, vol. 16, pp. 574–582, 1980.

Clause 10

[B10.1] Barringer, A.R. "The uses of audio and radio frequency pulses for terrain sensing," *Symposium Proceedings on Remote Sensing of the Environment*, Ann Arbor, MI, 1963.

[B10.2] Bogorodsky, V.V., Bentley, C.R., and Gudmandsen, P.E. *Radioglaciology*, Dordrecht, Netherlands: D. Reidel, 1985.

[B10.3] Bourgeois, J.M. and Smith, G.S. "A fully three-dimensional simulation of a ground-penetrating radar: FDTD theory compared with experiment," *IEEE Transactions on Geoscience and Remote Sensing*, vol. 24, pp. 36–44, Jan. 1996.

[B10.4] Daniels, D.J. *Surface Penetrating Radar*, Stevenage, London: Institution of Electrical Engineers, 1996.

[B10.5] Moghaddam, M., Yannakakis, E.J., and Chew, W.C. "Modeling of the subsurface interface radar," *Journal of Electromagnetic Waves and Applications*, vol. 5, pp. 17–39, 1991.

[B10.6] Spagnolini, U. "Permittivity measurements of multi-layered media with monostatic pulse radar," *IEEE Transactions on Geoscience and Remote Sensing*, vol. 35, pp. 454–463, 1997.

[B10.7] Turner, G. "Data processing techniques for the location of one dimensional objects using ground probing radar," *Exploration Geophysics*, vol. 20, pp. 379–382, 1989.

[B10.8] Turner, G., Siggins, A.F., and Hunt, L.D. "Ground penetrating radar – will it clear the haze at your site?" *Exploration Geophysics*, vol. 24, pp. 819–832, 1993.

For Further Reading

[B10.9] Daniels, D.J., Gunton, D.J., and Scott, H.F. "Introduction to subsurface radar," *Proceedings of the Institute of Electrical Engineers (U.K.)*, vol. 135, part F, pp. 278–320, 1988.

Clause 11

[B11.1] Moore, J.C. "High resolution dielectric profiling of ice cores," *Journal of Glaciology*, vol. 39, pp. 245–248, 1993.

[B11.2] Parasnis, D.S. *Mining Geophysics*, 2nd ed., Amsterdam: Elsevier, 1973, p. 163.

[B11.3] Telford, W.M., Geldart, L.P., Sheriff, R.E., and Keys, D.A. *Applied Geophysics*, London: Cambridge University Press, 1976, p. 448.

Clause 12

[B12.1] Browning, S.L. and Lodge, J.K. "Some techniques for determining the electromagnetic properties of lossy materials," *IEEE AP-S Workshop W3*, University of Washington, Seattle, June 24, 1994.

[B12.2] Collett, L.S. and Katsube, T.J. "Electrical parameters of rocks in developing geophysical techniques," *IEEE Transactions on Geoscience and Remote Sensing*, vol. 29, pp. 42–47, 1973.

[B12.3] Cook, J.C. "RF electrical properties of bituminous coal samples," *Geophysics*, vol. 35, pp. 1079–1085, 1970.

[B12.4] Levitskaya, T.M. and Sternberg, B.K. "Polarization processes in rocks I, complex dielectric permittivity method," *Radio Science*, vol. 31, pp. 755–779, Jul.–Aug. 1996.

[B12.5] Wilhelms, F., Kipfstuhl, J., Miller, H., Heinloth, K., and Firestone, J. "Precise dielectric profiling of ice cores: a new device with improved guarding and its theory," *Journal of Glaciology*, vol. 44, pp. 171–174, 1998.

Clause 13

[B13.1] Baker-Jarvis, J. "Transmission/Reflection and short-circuit line methods of measuring permittivity," *National Institute of Science and Technology Technical Note*, TN 1341, 1990.

[B13.2] Baker-Jarvis, J. and Junezic, M. "Analysis of open-ended coaxial probe with liftoff for non-destructive testing," *IEEE Transactions on Instruments and Measurements*, vol. 43, pp. 711–718, Oct. 1994.

[B13.3] Baker-Jarvis, J., Janezic, M., and Stafford, B. "Open-circuited holders for dielectric measurements of liquids and powders," *National Institute of Science and Technology Technical Note* IR5001, 1993.

[B13.4] Blackham, D. “Materials measurement using vector network analyzers,” Notes from Workshop W3, IEEE APS Symposium, University of Washington, Seattle, Jun. 1994.

[B13.5] Hewlett Packard, “HP 85070 A dielectric probe kit manual,” Product Note, Hewlett Packard, Inc., Palo Alto, CA (undated).

[B13.6] Nicolson, A.M. and Ross, G.F. “Measurements of the intrinsic properties of materials by time-domain techniques,” *IEEE Transactions on Instruments and Measurements*, vol. 19, no. 4, pp. 377–382, 1970.

[B13.7] Stuchly, M.A., Brady, M.M., Stuchly, S.S., and Gadja, G. “Equivalent circuit of an open ended coaxial line in a lossy dielectric,” *IEEE Transactions on Instruments and Measurements*, vol. 31, pp. 116–119, Jun. 1982.

[B13.8] Taherian, M.R., Yuen, D.J., Habashy, T.R., and Kong, J.A. “A coaxial-circular wave guide for dielectric measurement,” *IEEE Transactions on Geoscience and Remote Sensing*, vol. 29, no. 2, pp. 321–330, Mar. 1991.

[B13.9] Turner, G., Siggins, A.F., and Hunt, L.D. “Ground probing radar—will it clear the haze at your site?” *Exploration Geophysics*, vol. 24, pp. 819–832, 1993.

[B13.10] Ulaby, F.T., Dobson, M.C., and Brunfeldt, D. “Microwave probe for in-situ observations of vegetation dielectric,” *IEEE Instrumentation Measurement and Technology Conference,* Atlanta, GA, pp. 631–635, May 14–16, 1991.

Clause 14

[B14.1] Bhartia, P. and Hamid, M.A.K. “Dielectric measurements of sheet materials,” *IEEE Transactions on Instruments and Measurements*, vol. 22, no. 1, pp. 94–95, Mar. 1973.

[B14.2] Blackham, D. “Materials measurement using vector network analyzers,” Notes from Workshop W3, *IEEE APS Symposium*, University of Washington, Seattle, Jun. 1994.

[B14.3] Hoekstra, P. and Delaney, A. “Dielectric properties of soils at UHF and microwave frequencies,” *Journal of Geophysical Research*, vol. 79, pp. 1699–1708, 1974.

[B14.4] Maze, G., Bonnefoy, J.L., and Kamarei, M. “Microwave measurements of the permittivity using a sliding short-circuited wave guide method,” *Microwave Journal*, vol. 23, pp. 77–88, 1990.

[B14.5] Nelson, S.O., Stetson, L.E., and Schlaphoff, C.W. “A general computer program for precise calculation of dielectric properties from short circuited wave guide measurements,” *IEEE Transactions on Instruments and Measurements*, vol. 19, pp. 455–460, 1974.

[B14.6] Roberts, S. and von Hippel, A. “A new method for measuring permittivity and loss in the range of centimeter waves,” *Journal of Applied Physics*, vol. 17, pp. 610–616, 1946.

[B14.7] Somlo, P.I. “The exact numerical evaluation of the complex permittivity of a dielectric partially filling a wave guide,” *IEEE Transactions on Microwave Theory and Technology*, vol. 22, pp. 468–469, Apr. 1974.

[B14.8] Trasch, L.L., McLean, S.J., and Olsen, R.G. “Electromagnetic properties of dry and water saturated basalt rock, 1–110 GHz,” *IEEE Transactions on Geoscience and Remote Sensing*, vol. 36, pp. 754–766, May 1998.

Clause 15

[B15.1] Ghodgaonkar, D.K., Varadan, V.V., and Varadan, V.K. "A free-space method for measurement of permittivities and loss tangents at microwave frequencies," *IEEE Transactions on Instruments and Measurements*, vol. 37, pp. 789–793, 1989.

[B15.2] Kadaba, P.K. "Simultaneous measurement of complex permittivity and permeability in the millimeter region by a frequency-domain technique," *IEEE Transactions on Instruments and Measurements*, vol. 33, pp. 336–340, 1984.

[B15.3] Kavak, A., Vogel, W.J., and Xu, G. "Using GPS to measure ground complex permittivity," *Electronics Letters*, vol. 34, no. 3, pp. 254–255, Feb. 1998.

[B15.4] Lynch, A.C. "Precise measurements on dielectric and magnetic materials," *IEEE Transactions on Instruments and Measurements*, vol. 23, pp. 425–430, 1974.

[B15.5] Trasch, L.L., McLean, S.J., and Olsen, R.G. "Electromagnetic properties of dry and water saturated basalt rock, 1–110 GHz," *IEEE Transactions on Geoscience and Remote Sensing*, vol. 36, pp. 754–766, May 1998.

Clause 16

[B16.1] Afanas'ev, A.S., Belokudrenko, A.N., Garnaker'yan, A.A., Kachan, M.V., Mikhalko, M.M., Pimenov, S.F., Sushchii, S.M., and Entel, M.B. "Remote sensing of soils in the decametric range," *Soviet Journal of Remote Sensing*, vol. 8, no. 1, pp. 86–98, 1990.

[B16.2] Collins, M.J. and Livingstone, C.E. "On the dimensionality of multiparameter microwave image data from thin sea ice in the Labrador Sea," *IEEE Transactions on Geoscience and Remote Sensing*, vol. 34, pp. 114–136, Jan. 1996.

[B16.3] Haddad, Z.S., Dubois, P., and van Zyl, J.J. "Bayesian estimation of soil parameters from radar backscatter data," *IEEE Transactions on Geoscience and Remote Sensing*, vol. 34, pp. 76–82, 1996.

[B16.4] Kachan, M.V. and Pimenov, S.F. "Remote sensing of water salinity at decameter wavelengths," *IEEE Transactions on Geoscience and Remote Sensing*, vol. 35, no. 2, Mar. 1997.

[B16.5] Njoku, E.G. and Kong, J.A. "Theory for passive microwave remote sensing of near-surface soil mixture," *Journal of Geophysical Research*, vol. 82, pp. 3108–3118, 1977.

[B16.6] Oh, Y., Sarabandi, K., and Ulaby, F.T. "An empirical model and an inversion technique for radar scattering from bare soil surfaces," *IEEE Transactions on Geoscience and Remote Sensing*, vol. 30, pp. 370–381, Mar. 1992.

[B16.7] Raizer, V.Y., Zaitseva, I.G., Aniskovich, V.M., and Etkin, V.S. "Determining sea ice physical parameters from remotely sensed microwave data in the 0.3–18 cm band," *Soviet Journal of Remote Sensing*, vol. 5, pp. 29–42, 1986.

[B16.8] Reutov, E.A. and Shutko, A.M. "Prior-knowledge-based soil-moisture determination by microwave radiometry," *Soviet Journal of Remote Sensing*, vol. 5, pp. 100–125, 1986.

[B16.9] Schanda, E. "Microwave modeling of snow and soil," *Journal of Electromagnetic Waves and Applications*, vol. 1, pp. 1–24, 1987.

For Further Reading

[B16.10] Moore, R.K. "Active microwave systems," in Lintz, J. and Simonett, D.S. (ed.), *Remote Sensing of the Environment*, Reading, MA: Addison-Wesley, 1976, Chapter 7.

[B16.11] Special Issue on Remote Sensing, *IEEE Transactions on Geoscience and Remote Sensing*, vol. 30, no. 2, 1992.

[B16.12] Tsang, L., Kong, J.A., and Shin, R.T. *Theory of Microwave Remote Sensing*, New York: Wiley, 1985.

[B16.13] Ulaby, F.T., Moore, R.K., and Fung, A.K. *Microwave Remote Sensing, Active and Passive*, vols. 2 and 3. Norwood, MA: Artech House, 1986.

